JACS
JOURNAL OF THE AMERICAN CHEMICAL SOCIETY
pubs.acs.org/JACS
Article

Deciphering the Phillips Catalyst by Orbital Analysis and Supervised Machine Learning from Cr Pre-edge XANES of Molecular Libraries

David Trummer, Keith Searles, Alexander Algasov, Sergey A. Guda, Alexander V. Soldatov, Harry Ramanantoanina, Olga V. Safonova,* Alexander A. Guda,* and Christophe Copéret*

Cite This: https://doi.org/10.1021/jacs.0c10791
Read Online

ABSTRACT: Unveiling the nature and the distribution of surface sites in heterogeneous catalysts, and for the Phillips catalyst (CrO_3/SiO_2) in particular, is still a grand challenge despite more than 60 years of research. Commonly used references in Cr K-edge XANES spectral analysis rely on bulk materials (Cr-foil, Cr_2O_3) or molecules ($CrCl_3$) that significantly differ from actual surface sites. In this work, we built a library of Cr K-edge XANES spectra for a series of tailored molecular Cr complexes, varying in oxidation state, local coordination environment, and ligand strength. Quantitative analysis of the pre-edge region revealed the origin of the pre-edge shape and intensity distribution. In particular, the characteristic pre-edge splitting observed for Cr(III) and Cr(IV) molecular complexes is directly related to the electronic exchange interactions in the frontier orbitals (spin-up and -down transitions). The series of experimental references was extended by theoretical spectra for potential active site structures and used for training the Extra Trees machine learning algorithm. The most informative features of the spectra (descriptors) were selected for the prediction of Cr oxidation states, mean interatomic distances in the first coordination sphere, and type of ligands. This set of descriptors was applied to uncover the site distribution in the Phillips catalyst at three different stages of the process. The freshly calcined catalyst consists of mainly Cr(VI) sites. The CO-exposed catalyst contains mainly Cr(II) silicates with a minor fraction of Cr(III) sites. The Phillips catalyst exposed to ethylene contains mainly highly coordinated Cr(III) silicates along with unreduced Cr(VI) sites.

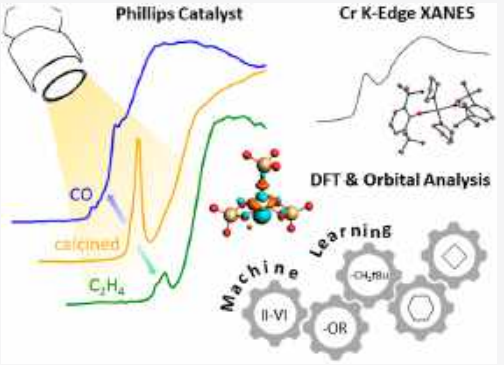

INTRODUCTION

The Phillips catalyst, based on silica-supported Cr oxide (CrO_3/SiO_2), is currently responsible for 30−40% of the world production of high-density polyethylene.[1] Despite its implementation for more than 60 years, the identification of surface and active sites has remained a challenge and a highly debated topic.[2] X-ray absorption spectroscopy (XAS) has received significant attention as a spectroscopic means to elucidate the structure of these sites.[2i,3] Nevertheless, understanding the spectroscopic signature of chromium surface sites is challenging because of their unusual structural features.[4] Commonly used reference materials for comparative XAS analysis, such as Cr foil, bulk oxides, and chlorides, greatly differ from actual surface sites in terms of geometry and the nature of ligands attached to Cr. Therefore, obtaining insight into fundamental factors affecting the Cr K-edge XAS is critical for developing meaningful structure−activity relationships.

X-ray absorption near-edge structure (XANES) studies on supported Cr(VI) oxides report a gradual shift of the Cr K-edge position to lower energy upon contact with ethylene. In parallel, the intense pre-edge feature typical for pseudotetrahedral chromates is gradually replaced by two weak bands which were assigned to the formation of reduced Cr species, specifically Cr(II) sites, with oxygenated ethylene byproducts coordinated to Cr.[3e,f,h,i,5] This process is further complicated by the fact that, after the induction period, the Cr(II) sites are proposed to reoxidize to Cr(III) under reaction conditions,[2a,h,6] so that both Cr(II) and Cr(III) sites are proposed as key intermediates. Figure 1 left illustrates significant changes in the pre-edge and edge region of the Cr K-edge XANES spectra of the Phillips catalyst, which are typically obtained at three different stages of activation:[1b,2h,3d,i,5a,7] P1, after calcination; P2, after prereduction with CO; and P3, after calcination and ethylene exposure at 110 °C. In parallel, XAS studies focusing on olefin oligomerization show that the shapes of Cr K-edge XANES spectra are highly sensitive to the local environment and the ligand donor strength. In a series of Cr molecular complexes varying in ligand environment and L-type ligands,[8] octahedrally coordinated $CrCl_3(L)_x$ complexes with P-, S-, or N-type ligands

Received: October 18, 2020

https://doi.org/10.1021/jacs.0c10791
J. Am. Chem. Soc. XXXX, XXX, XXX−XXX

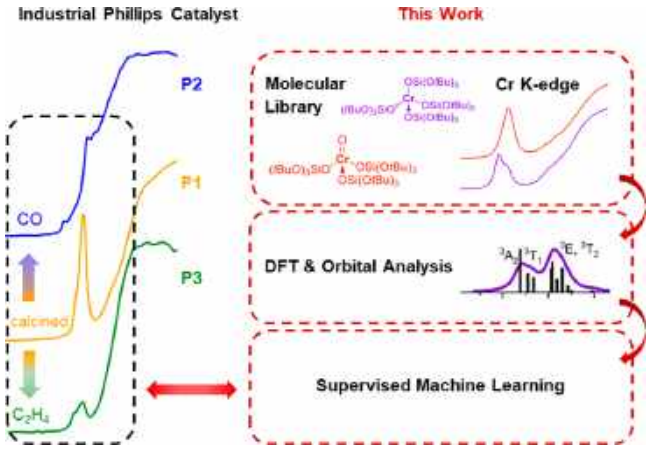

Figure 1. (Left) Typical experimental Cr K-edge XANES spectra of the Phillips catalyst at three different stages of the process. P1, after calcination; P2, after prereduction with CO; P3, after calcination and ethylene exposure at 110 °C. All raw data were kindly provided by Groppo and collaborators as originally published.[5a] (Right) Three-step strategy of this work to decipher the information content in the pre-edge structure of the Phillips catalyst.

in facial or meridional coordination environments show significant differences in edge energies.

However, the sole use of the absorption edge energy for calibration can sometimes be ambiguous: Mn(III) and Mn(V) complexes can have similar absorption edge positions when exchanging an azide ligand in Mn(III) to a nitrido ligand in Mn(V) complexes.[9] Several studies on other 3d metals also show that pre-edge features are greatly affected by structural parameters and oxidations states.[10]

Taking advantage of the high structural sensitivity of the pre-edge shape in 3d metals, Wilke et al. established, already two decades ago, an empirical methodology to extract structural information from pre-edge features, where both the oxidation state and the coordination number of Fe could be classified.[11] These examples illustrate that pre-edge and near-edge XANES features for 3d elements contain a lot of structural information. However, the methods for analysis are still not ideal due to the lack of theoretical background knowledge. Another limitation, for Cr, is the lack of advanced molecular reference materials, which makes it difficult to unambiguously assign highly dispersed Cr surface species in the Phillips catalyst.

With the goal to decipher the nature of surface species in the Phillips catalyst, we propose that an in-depth analysis of the pre-edge and the Cr K-edge XANES spectra, obtained from a series of tailored molecular complexes, would help to establish a molecular-level understanding of the spectroscopic signatures of Cr surface sites. Therefore, we first developed a series of tailored molecular Cr complexes with a broad range of oxidation states—Cr(II) to Cr(VI)—and coordination environments. While focusing mainly on oxygen-based ligands due to their similarity to the expected surface species, additional types of structures are also examined to probe the effect of the ligand σ-donor strength. XANES spectra of this series of molecular Cr complexes are recorded at the K-edge and compared to DFT simulations to carry out an in-depth orbital analysis and to establish relationships between electronic structures and pre-edge signatures. Further theoretical calculations address possible active sites and reaction intermediates that can be encountered on surfaces, but whose coordination environments are not readily obtained via molecular chemistry. To improve the quality of the analysis and estimate possible uncertainties, we rely on supervised machine learning (ML) which was recently applied to a range of challenges covered by XAS.[12] We reduced the dimensionality of the XANES spectra by selecting appropriate descriptors and the algorithm based on decision trees that was trained to predict oxidation states, interatomic distances, and types of ligands. The concept of descriptors allowed the calibration of systematic differences between calculations and experimental spectra based on the reference database of molecular complexes. Supervised ML and linear combination fitting allowed us to decipher the oxidation state for unknown mixtures of Cr surface species in the industrial Phillips catalyst at three different stages of activation, as shown in Figure 1.[1b,2h,3d,i,5a,7]

RESULTS AND DISCUSSION

Synthesis and Structure of Molecular Cr Complexes.

To mimic potential surface and active site structures in the Phillips catalyst, we focused on developing tailored, low-coordinate, and monomeric Cr(II−VI) tris-*tert*-butoxysiloxide complexes that can serve as a surrogate for surface siloxide ligands (see Figure 2A). Since Cr(II) tris-*tert*-butoxysiloxide complexes are dimeric,[13] we used 2,6-di-*tert*-butoxyphenoxide ligands in the presence of THF to obtain a monomeric $[Cr(tBu_2PhO)_2(THF)_2]$ complex [**II.1**] in exclusively oxygen environments. A similar approach with 4-methyl-2,6-di-*tert*-butoxyphenoxide ligands is reported in the open literature.[14] In addition, the monomeric $[Cr(acac)_2]$[15] complex [**II.2**] and the dimeric $[Cr(\mu\text{-}OSi(OtBu)_3)(OSi(OtBu)_3)]_2$[13] complex [**II.3**] were synthesized as a benchmark for the tris(*tert*-butoxysiloxide) series. In contrast to the rather rare, monomeric Cr(II) complexes, Cr(III) siloxide and alkoxide based complexes are well established in the literature. In addition to the square-pyramidal $[Cr(OSi(OtBu)_3)_3]$ complex [**III.1**], the trigonal-bipyramidal $[Cr(OSi(OtBu)_3)_3THF_2]$[16] complex [**III.2**] was synthesized to investigate changes in the pre-edge as a function of the local environment. A more tetrahedral-like environment for the Cr(III) formal oxidation state $[(K^+K\text{-}222)(Cr^-(OSi(OtBu)_3)_4)]$ [**III.3**] was obtained by reacting $[K^+(Cr^-(OSi(OtBu)_3)_4)]$[17] in the presence of Kryptofix-2,2,2 (K-222). The octahedrally coordinated $[Cr(OCHMeCH_2OMe)_3]$[18] complex [**III.4**] was chosen as a representative molecule with O_h symmetry. With respect to potential active site structures in Cr-based ethylene polarization, the trigonal $[Cr(CHSiMe_2)_3]$[19] alkyl complex [**III.5**] was synthesized and included in the XANES analysis.

We broadened the substrate scope for Cr(III) complexes by including the square-pyramidal $[Cr(OSi(OtBu)_3)_3DME]$ complex [**III.6**] and the pseudo-octahedral polyhederal-oligosilsesquioxane $[(cC_5H_9)_7Si_7O_9(O)_3Cr(THF)_3]$ complex [**III.7**]. We completed the Cr(III) series by the analysis of the already known $[Na(Cr(OSi(OSi(OtBu)_3)_4)]$[17] [**III.8**], $[Cr(acac)_3]$ [**III.9**], and the dimeric $[o\text{-}(Cr(OSiOtBu_3)_2)_2]$[13] [**III.10**] complexes. We included $[Cr_2O_3]$, a classical reference compound, into the Cr(III) series to benchmark with previous studies. The series of Cr(IV) molecular complexes includes $[Cr(OSi(OtBu)_3)_4]$ [**IV.1**], the isostructural $[Cr(OtBu)_4]$[20] [**IV.2**], and the corresponding Cr-alkyl complex $[Cr(CH_2tBu)_4]$[21] [**IV.3**] in order to analyze changes in the Cr K-edge and pre-edge structure with increasing σ-donating ability of ligands in the absence of changes in the local environment.

The mono-oxo $[Cr{=}O(OSi(OtBu)_3)_3]$ complex [**V.1**] and the dioxo $[Cr{=}O_2(OSi(OtBu)_3)_2]$ complex [**VI.1**] are

https://doi.org/10.1021/jacs.0c10791
J. Am. Chem. Soc. XXXX, XXX, XXX−XXX

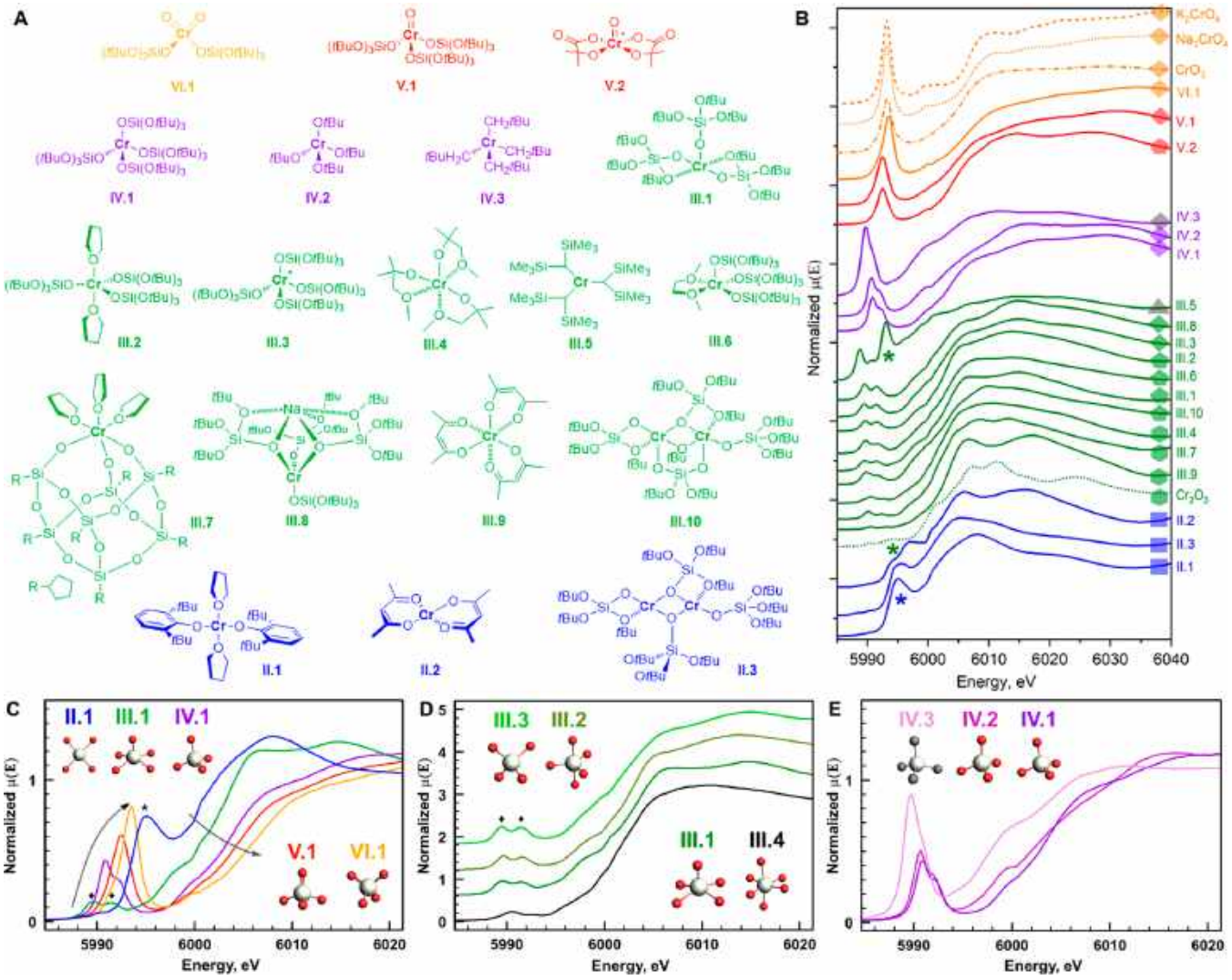

Figure 2. (A) Molecular Cr(II−VI) complexes investigated experimentally in this work. (B) Experimental Cr K-edge XANES spectra of the series of crystalline reference complexes. Complex **II.1** and **III.5** display an intense shoulder (*) before the rising edge. Note that Cr_2O_3 shows a similar shoulder (*) in the pre-edge that arises from Cr−O−Cr long-range interactions and should therefore not be used as a reference for Cr(III) molecular complexes (see Figure S14). (C) XANES spectra for selected molecular Cr complexes **II.1**−**VI.1**. Arrows indicate shifts of both the K-edge and pre-edge toward higher energy. Complex **II.1** displays the intense shoulder (*) before the rising edge, and complex **III.1** shows a characteristic splitting (♦) in the pre-edge. (D) Effects of ligand field changes on the pre-edge shape and intensity in **III.1**−**III.4**. The appearance of the weak pre-edge feature in the formally octahedral complexes **III.4** (and **III.7**) is due to quadrupole transitions accompanied by small dipole contributions from distorted centrosymmetric ligand fields. All complexes show the characteristic pre-edge splitting (♦) independent of the ligand field. (E) Effects of the ligand *σ*-donor strength on the edge and pre-edge features of tetrahedrally coordinated Cr(IV) complexes **IV.1**−**IV.3**. Strongly *σ*-donating alkyl ligands show lower edge energies and higher pre-edge intensities.

developed as representative molecules of the Cr(V) and Cr(VI) formal oxidation states, respectively.

The square-pyramidal $[Na(Cr{=}O(CO_2CMe_2O)_2]$[22] complex [**V.2**] and the classical Cr(VI) reference compounds [Na_2CrO_4] and [K_2CrO_4] were additionally measured to extend the analysis of the Cr-XANES spectra for high oxidation states. Details regarding the synthesis and the characterization, including X-ray crystallography, are described in the SI.

Qualitative Description on Changes in Spectroscopic Features of Cr K-Edge XANES Spectra. Figure 2B displays the series of XANES spectra of synthesized and commercially available reference compounds. Figure 2C shows selected XANES spectra of molecular complexes in the range of Cr(II)−Cr(VI) oxidation states. The increase in oxidation state results in a shift of the rising edge to higher energy from 5999 to 6006 eV. The square-planar complex **II.1** shows negligible pre-edge intensities below 5992 eV and a remarkably intense shoulder with a maximum at 5995.3 eV (marked with *) before the rising edge. This shoulder can be erroneously attributed to the pre-edge if compared to the Cr(VI) complex, but it originates mainly from a 1s to $4p_z$ transition as discussed later in the next section. Such a shoulder is also marked for complex **III.5** with a planar geometry.

Pre-edge intensity increases along with the oxidation state as well as for tetrahedral-like geometries in **IV.1**−**VI.1**. Complex **VI.1** displays the most intense pre-edge (Figure 2C). Complexes **III.1** and **IV.1** show a characteristic splitting in their pre-edge structure (indicated with ♦) that unites into a single intense feature in **V.1** and **VI.1**. This feature is strikingly pronounced for

https://doi.org/10.1021/jacs.0c10791
J. Am. Chem. Soc. XXXX, XXX, XXX−XXX

all examined Cr(III) complexes, regardless of the choice of the ligand and the local environment.

To investigate the impact of the local environment on the pre-edge structure, we compare four Cr(III) complexes. As indicated in Figure 2D, the octahedral (O_h) **III.4**, square-base pyramidal (C_{4v}) **III.1**, trigonal-bipyramidal (D_{3h}) **III.2**, and tetrahedral (T_d) **III.3** complexes show a characteristic splitting in their pre-edge structure independent of the local environment. The pre-edge intensity is the lowest in the octahedral **III.4** complex, whereby both the intensity and the pre-edge splitting are more pronounced in the square-pyramidal complex **III.1** and the tetrahedral complex **III.3** when geometry deviates from centrosymmetric coordination. Cr_2O_3 also displays a shoulder in the pre-edge region, which can be misinterpreted as a pre-edge splitting. However, the origin of this feature arises from nonlocal pre-edge transitions mediated by Cr−O−Cr configurations and cannot be compared to molecular complexes (see Figure S14).[23]

The third important effect, influencing the edge position and the pre-edge shape, is the σ-donating ability of the ligands. We investigated this influence on the Cr K-edge by comparing XANES spectra of three tetrahedral Cr(IV) complexes with siloxide (**IV.1**), alkoxide (**IV.2**), and alkyl (**IV.3**) ligands. As indicated in Figure 2E, complex **IV.1**, with the least σ-donating ligand, shows the highest edge energy. *tert*-Butyl alkoxide ligands are slightly more σ-donating (basic), resulting in a small shift in the Cr K-edge of 0.1 eV to lower energy. Complex **IV.3**, surrounded by four neopentyl ligands, shows a by far greater ligand influence. Such strongly σ-donating alkyl ligands form covalent Cr−C bonds and lower the rising edge position by more than 2.4 eV compared to complex **IV.1**. The shift to lower edge energy from complex **IV.1** to **IV.3** is accompanied by a significant increase in the overall pre-edge area. Increasing the p-content with the covalency of the Cr−C bond in **IV.3** allows a more efficient p−d mixing in the tetrahedral ligand field. This explains the increase in the pre-edge area.

In conclusion, this tailored series of molecular Cr complexes highlights how subtle differences in both formal oxidation state of the absorbing atom, local symmetry, and ligand type greatly affect the shape and intensity of the pre-edge. The mutual influence of the d-electron count at Cr and the σ-donating properties of the surrounding ligands makes a detailed analysis of the pre-edge features indispensable. In the following section, we will focus on the theoretical molecular orbital analysis to explain the shape and intensity distribution of pre-edge features in the Cr K-edge XANES spectra.

Molecular Orbital Understanding of the Pre-Edge Features of Cr K-Edge XANES Spectra. 3d metals are characterized by strong electron−electron correlations in the localized d-shell. For the Phillips catalyst, the range of proposed catalytically active oxidation states of Cr varies from Cr(II) to Cr(VI), thus covering d^4 to d^0 ground state configurations or $1s^13d^5$ to $1s^13d^1$ excited state configurations. The variation of the pre-edge shape across the excited state configurations is demonstrated via two approaches. Namely, Figure 3A and B are based on many-body multiplet simulations where all structure-related parameters were fixed either to the tetrahedral or octahedral coordination, with variable electron count in the d-shell. Figure 5 is based on the one-electron DFT approach, which underestimates electron−electron correlations but accounts for the real structure of the complex and provides intuitively clear assignments for each transition. The combined approach is demonstrated in Figure 3C.

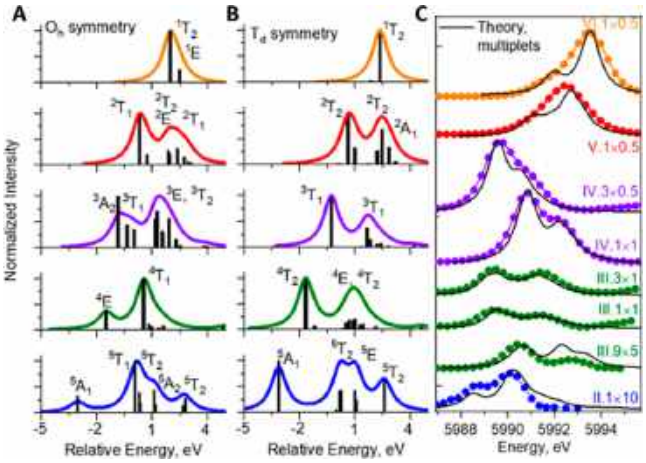

Figure 3. (A, B) Idealized multiplet calculations for Cr(II)−Cr(VI) ions in the octahedral and tetrahedral crystal field with 0.5 eV strength. Term symbols are assigned for the most intense transitions according to their $1s^13d^{n+1}$ electronic configuration. To account for covalency effects, the amplitudes for the transition matrix elements were estimated from DFT calculation of tetrahedral $(Cr(OH)_4)^{2+}$ and octahedral $(Cr(H_2O)_6)^{6+}$ model complexes (see Tables S8−S10). (C) Ligand field multiplet calculations for selected and experimentally measured (symbols) complexes.

In Figure 3A and B, we simulated the transition probabilities for the multiplets arising from $1s^13d^{n+1}$ electronic configurations in idealized tetrahedral and octahedral Cr coordination spheres. The typical values for the crystal field energies of molecular complexes are 0.5−1.0 eV. We found that this parameter has minor effects on the shape of the calculated spectra. Therefore, only calculations for 0.5 eV are shown. Such model simulations are useful to assign the most intense transitions according to their term symbols without spin−orbit coupling. We found that high-spin states are lower in energy for all configurations under study (see Tables S11 and S12). Only quadrupole transitions have nonzero intensities in the case of O_h symmetry (Figure 3A). The tetrahedral complexes display both quadrupole and dipole transitions (Figure 3B), the latter being triggered by an admixture of Cr 4p into 3d orbitals. For the empty 3d-shell of Cr(VI), only two transitions are expected, corresponding to the 2-fold and 3-fold degenerate molecular orbitals (e_g and t_{2g} in O_h and e and t_2 in T_d). These two transitions, $^1T_2$ and ^1E in the octahedral symmetry, are separated by a crystal field. The relative intensity is determined by the degeneracy of the states and the hybridization of 3d and ligand orbitals, i.e., the covalency. In the tetrahedral field the t_2 states are hybridized with Cr 4p states and only one strong dipole transition ($^1T_2$) dominates in the calculated spectrum. For lower oxidation states, Cr(III)−Cr(V), the pre-edge transition consists of two well-separated groups of multiplets. The energy splitting between them increases with the number of unpaired electrons in the d-shell due to stronger electron−electron exchange interactions and becomes largest for the $1s^13d^5$ electronic configuration in Cr(II). The lowest energy transition in Cr(II), for both T_d and O_h geometries, is a $^5A_1$ many-electron state. In this case, the value for the orbital momentum is zero, due to the single occupation of all possible d-states in the excited state configuration.

The real complexes in our library are distorted from ideal tetrahedral or octahedral symmetry and contain up to 100 atoms. In Figure 3C we use a ligand field DFT (LFDFT)

https://doi.org/10.1021/jacs.0c10791
J. Am. Chem. Soc. XXXX, XXX, XXX−XXX

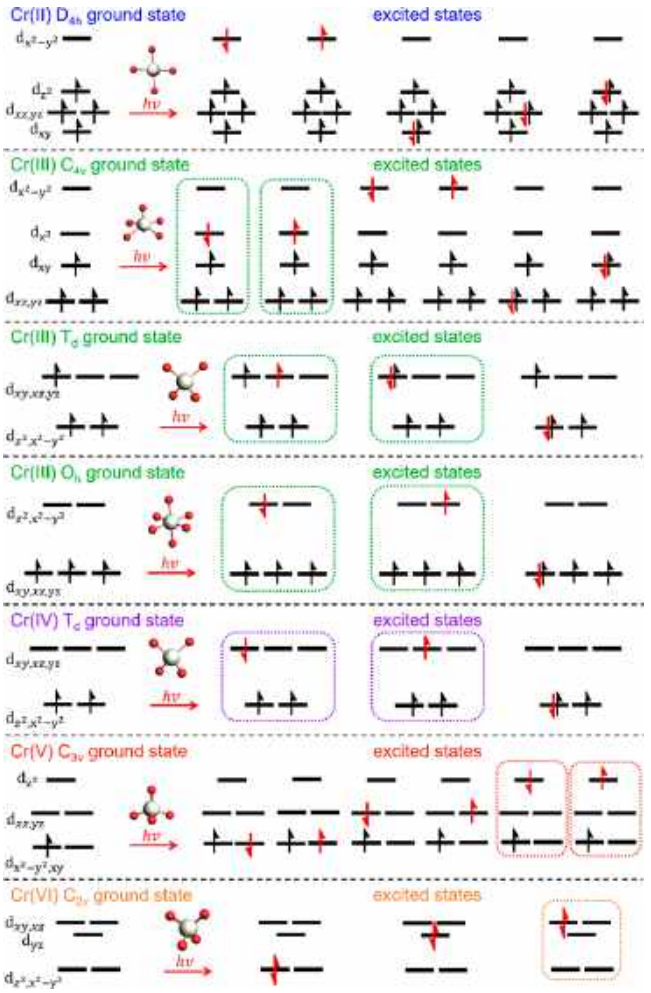

Figure 4. Simplified representation of molecular orbital diagrams and 1s−3d transitions for selected ideal geometries and Cr oxidation states. The most intense transitions are outlined in colors.

method,[24] a model Hamiltonian concept operated on top of a DFT calculation. It allows obtaining nonempirically all the important parameters (Slater−Condon integrals, spin−orbit coupling constants, and ligand-field potentials) for the calculation of pre-edge structures. A good agreement between experimental and calculated spectra is observed for the relative intensities of the pre-edge features and their splitting. For the tetrahedral **III.3**, **IV.1**, and **IV.3** complexes the LFDFT approach is consistent with the parametrized crystal field calculations in Figure 3B. In the experimental spectrum of the octahedral complex **III.9** ($Cr(acac)_3$) the first pre-edge feature is of higher intensity than the second one. The opposite behavior is observed in the crystal field calculations (green curve in Figure 3A). This difference is explained by a difference in covalency in the Cr−O bonds of **III.9** and the model complex $(Cr(H_2O)_6)^{6+}$, which was used to estimate amplitudes for the transition matrix elements in the multiplet simulations.

For the assignment of the pre-edge features in terms of chemically relevant molecular orbitals, we rely on the B3LYP density functional level of theory ~~as demonstrated in~~ Figures 5 and ~~Figure 8~~. Pre-edge spectral features in Cr K-edge XANES spectra originate from quadrupolar 1s−3d transitions that significantly gain in intensity when symmetry-allowed p−d mixing occurs. Such transitions thus depend on the local geometry (ligand field) and the d^n electronic configuration of Cr. One-electron levels for selected ideal geometries with different oxidation states are shown in Figure 4. Empty molecular orbitals can accept 1s electrons in both α and β spin states, while only transitions from the α (or β) 1s electron are allowed for half-filled orbitals. For an empty d-shell (d^0 electronic configuration, Cr(VI)), α/β transitions are energetically equivalent, thus reflecting the energy splitting of the 3d shell imposed by the ligand field. The pre-edge feature gains in complexity due to spin-exchange interactions between unpaired electrons in Cr(V−II) complexes with a d$^{1-4}$ ground electronic configuration.[25] Namely, a splitting of the pre-edge up to several eVs can be observed as a result of parallel or antiparallel spin orientations between an excited 1s electron and the unpaired 3d electrons.

Figure 5 provides an overview of the dominant 1s to 3d and 4p transitions that contribute to the shape of the pre-edge. The intensities of the colored bars represent the Mulliken population of molecular orbitals multiplied by the transition probability. The d-states are further attributed to orbital momentum projections, while all the other contributions are marked as s and p in the graph. Separate β spin state contributions are indicated with a negative sign in the ground state Mulliken population. Due to bulky ligands most of the molecular complexes or surface sites have a generally low symmetry, thus preventing the assignment to a specific point group of high-symmetry point group.

Molecular orbitals with a dominant contribution to the pre-edge shape and intensity are visualized on the right side in Figure 5A−F. The formally Cr(II), d^4 complex, **II.1**, shows weak pre-edge intensities below 5992 eV due to the inversion symmetry which prohibits 4p−3d orbital mixing in an ideal square-planar geometry. Instead, a remarkably intense shoulder appears on the rising edge. As shown in Figure 5A, the main d-contributions to the shape of the pre-edge arise from the 1s α-transition to the empty d_{x2-y2} (A) and the 1s β-transition to the half-filled d_{z2} (B) orbital. The broad intense shoulder (consisting of C, D, and E) originates from 1s to $4p_z$ transitions. The remaining 1s β-transitions to the half-filled d_{xy} and d_{xz} orbitals and the empty d_{x2-y2} orbital are hidden in C and D. Generally, pre-edge intensities increase when geometry deviates from centrosymmetric coordination. The pre-edge of the square-pyramidal-like d^3 complex **III.1** is dominated by two main transitions (A, B) that are ca. 1.3 eV apart (Figure 5B). Assuming an ideal square-pyramidal geometry, the A and B peaks correspond to the spin up (α) and spin down (β) transitions from the 1s to the same antibonding d_{z2}/p_z orbitals (see Figure 4, Cr(III) C_{4v} symmetry). The pre-edge splitting in Cr(III) complexes thus reflects the spin-exchange interaction between excited 1s electrons and the d^3 electronic configuration. The weak transition near A and B originates from α/β d_{x2-y2} orbitals and the three singly occupied β-orbitals (d_{xy}, d_{yz}, d_{xz}).

Complex **III.3** has a pseudo-tetrahedral geometry, which allows 3d−4p mixing for the t_2 set (d_{xz}, d_{xy}, d_{yz} orbitals). The pre-edge shape consists of two spin-pairs: A,C and B,D are associated with α/β-transitions to the two empty orbitals of the t_2 set. The observed exchange splitting is ca. 1.4 eV (Figure 5C). The additional β-transitions have lower intensity and are associated with the half-filled d_{x2-y2} and d_{z2} orbitals. The absence of inversion symmetry is responsible for the characteristically intense pre-edge feature, while the presence of one unpaired electron in the t_2 orbitals reduces the intensity as compared to the tetrahedral Cr(IV) complexes.

https://doi.org/10.1021/jacs.0c10791
J. Am. Chem. Soc. XXXX, XXX, XXX−XXX

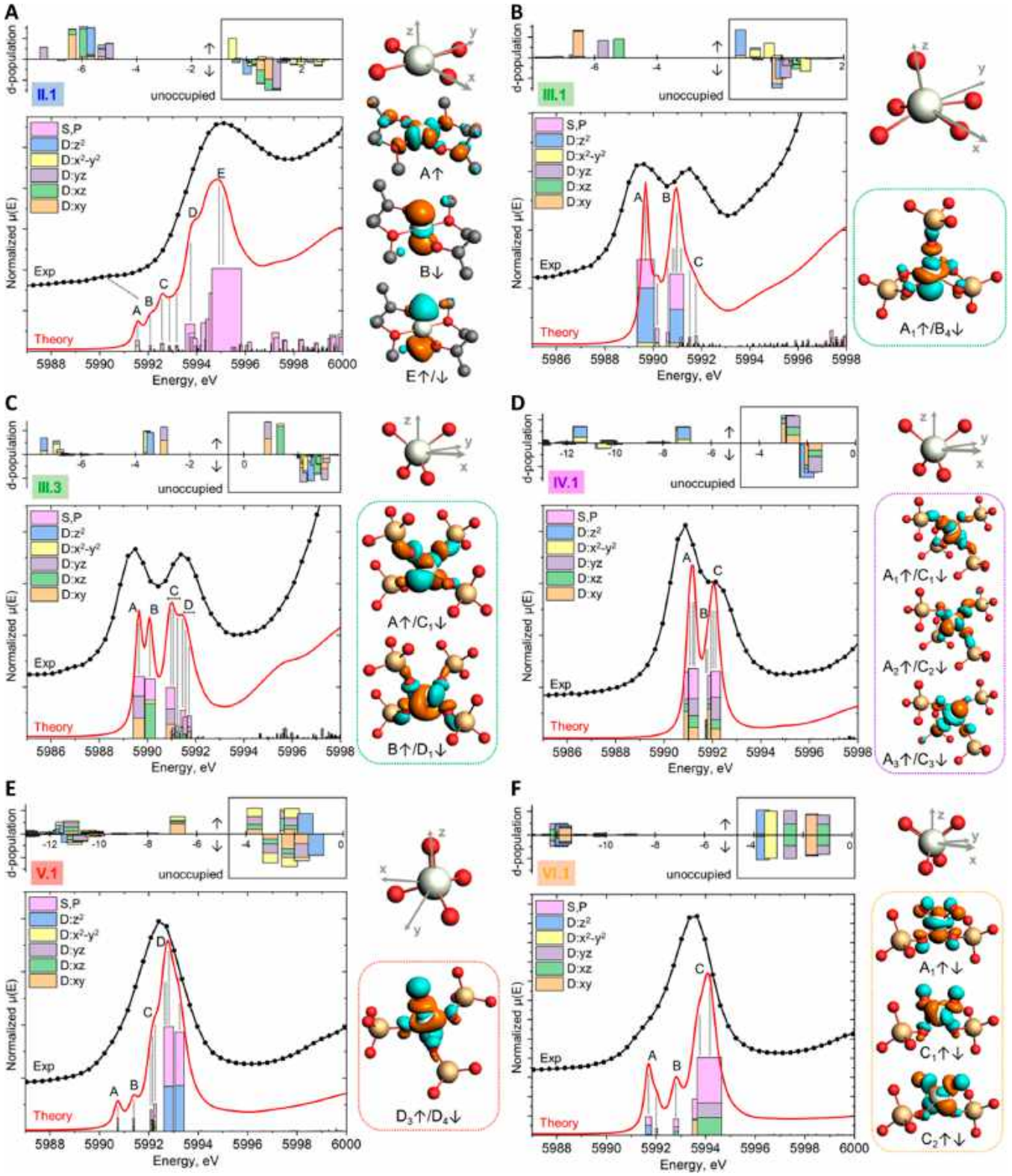

Figure 5. Experimental (black) and calculated (red) pre-edge spectra for selected Cr complexes. The intensities of the colored bars represent the Mulliken population of d and p orbitals multiplied by their transition probabilities. The widths of the colored bars are proportional to the amplitudes of the transitions. The ground state Mulliken populations of d states with separate contributions from α and β spin states are visualized above each spectrum. The x-axis corresponds to the photon energy, while the orbital energy eigenvalues are used for the Mulliken population analysis. Selected molecular orbitals with dominant contributions to the pre-edge intensity are visualized on the right side of each panel. Despite the high symmetry of the first coordination sphere, several colored bars contain formally prohibited transitions in panels A−F due to the lower overall symmetry of the molecular complexes.

https://doi.org/10.1021/jacs.0c10791
J. Am. Chem. Soc. XXXX, XXX, XXX−XXX

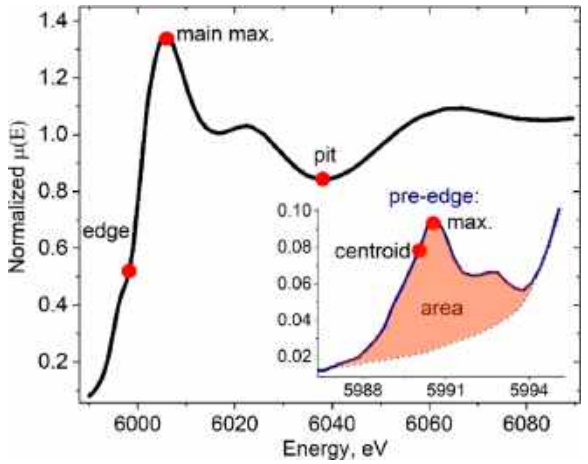

Figure 6. Visual representation of the pre-edge and near-edge descriptors that are used for the ML and linear combination analysis. The chosen descriptors for the X-ray absorption fine structure are related to specific physical phenomena; for example, the edge position is affected by the combination of the Cr oxidation state, the donor/acceptor properties of the ligands, and the contraction/elongation of the first coordination sphere (see Section 4.1 of the SI). Additional XANES descriptors are discussed in Section 4.2 of the SI.

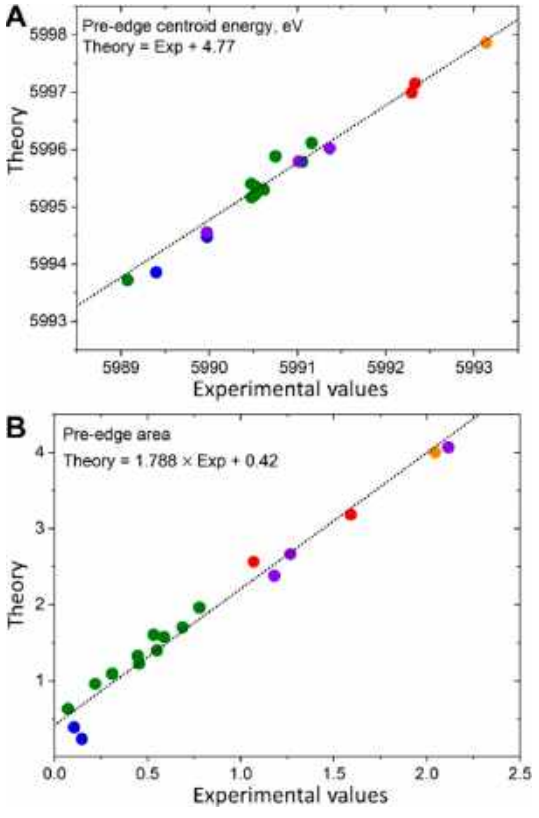

Figure 7. Calculated pre-edge areas and pre-edge centroid energies are compared to the values obtained from experimental spectra in Figure 2B. The dotted line shows a linear fit to establish a calibration of theoretical values with respect to experimental ones. Complex **II.2** is omitted from the calibration since this complex contains close layers of planar molecules in the crystal packing that will affect the experimental spectrum, while interlayer interactions are not accounted for the calculations.

The Cr(IV) complexes with a d^2 electronic configuration have one less unpaired electron, leading to a smaller exchange splitting of the two pre-edge features. In **IV.1**−**VI.3** with Cr in an almost tetrahedral coordination sphere, two electrons occupy the half-filled e orbitals, while the t_2 orbitals are vacant. The pre-edge intensity is dominated by 1s to t_2 transitions, which are separated by ca. 1 eV for α/β spins (peaks A, C in Figure 5D). The two weak β-transitions (peak B) correspond to the half-filled d_{x2-y2} and d_{z2} orbitals of the e set. The energy difference between the two sets of β-transitions, B and C, represent the t_2 to e crystal field splitting energy in the tetrahedral ligand field.

Complex **V.1** (Figure 5E) is characterized by the formally C_{3v} local symmetry and a d^1 electronic configuration. The α/β transitions D_3 and D_4 originate from the d_{z2} orbital hybridized with p_z orbitals of the nearest apical oxo ligand and dominate the pre-edge intensity due to the efficient 4p−3d mixing. The smaller energy splitting between spin-paired transitions D_3 and D_4 is explained by the presence of only one unpaired electron in the ground state electronic configuration. Other weak peaks, labeled as A, B, C, and D_1, arise from transitions to hybridized d orbitals from π contributions to the Cr═O bond, predominantly from the d_{xz} and d_{yz} orbitals.

The C_{2v} symmetrical complex **VI.1**, with an empty d-shell, shows five energy levels in the pre-edge with energetically equivalent α/β electronic transitions (Figure 5F). The quasi-degeneracy of the d_{x2-y2}, d_{z2} and the d_{xy}, d_{xz} orbitals leads to three sets of electronic transitions labeled as A, B, and C. The dominant contribution to the pre-edge intensity arises from the orbitals with σ character (d_{xz}, d_{yz}) of the Cr═O bonds.

The calculations displayed in Figure 5 show small differences in relative intensities and exchange splitting when compared to the LFDFT approach in Figure 3C. However, Figure 5 justifies the use of one-electron DFT calculations for a correct estimation of the pre-edge energies and areas. Further quantitative analysis is based on these two parameters of the pre-edge, which are easily accessible from any modern quantum chemistry software.

Classification of the Oxidation State and the Local Cr Environment by Using XANES Descriptors and ML Algorithms. We designed our library of XANES spectra with the objective to unveil the site distribution on silica including the identification of catalytically active sites. In a common fingerprint approach, the XANES spectrum of the Phillips catalyst at every stage of the process is described by one of the reference structures from the library with the highest similarity. Since a molecular library cannot cover the full range of expected parameters (oxidation state, geometry, coordination number, metal−ligand bond strength, type of ligand, etc.), an interpolation between reference points is required. This task can be efficiently solved by means of ML algorithms, which use a data set of reference spectra for training. This is an elegant way to solve classification problems. In such a way, the local coordination motifs for a given experimental XANES spectrum can be predicted based on the theoretical training set of several hundreds of thousands of structures, e.g., from a Materials Project.[12a] Similarly, principle components of the reference data set can be used as descriptors to discriminate between local coordination environments[12d] and the type of ligands.[12b] Neural network is a recognized tool to analyze complex data sets, but its practical application requires a huge number of entries in the training set.[26] Commonly, most studies are restricted to a few high-quality experimental references extended by representative theoretical models. This is a small database of high dimensional objects, since each XANES spectrum contains around 100 points. To improve the efficiency of ML algorithms, we reduce

https://doi.org/10.1021/jacs.0c10791
J. Am. Chem. Soc. XXXX, XXX, XXX−XXX

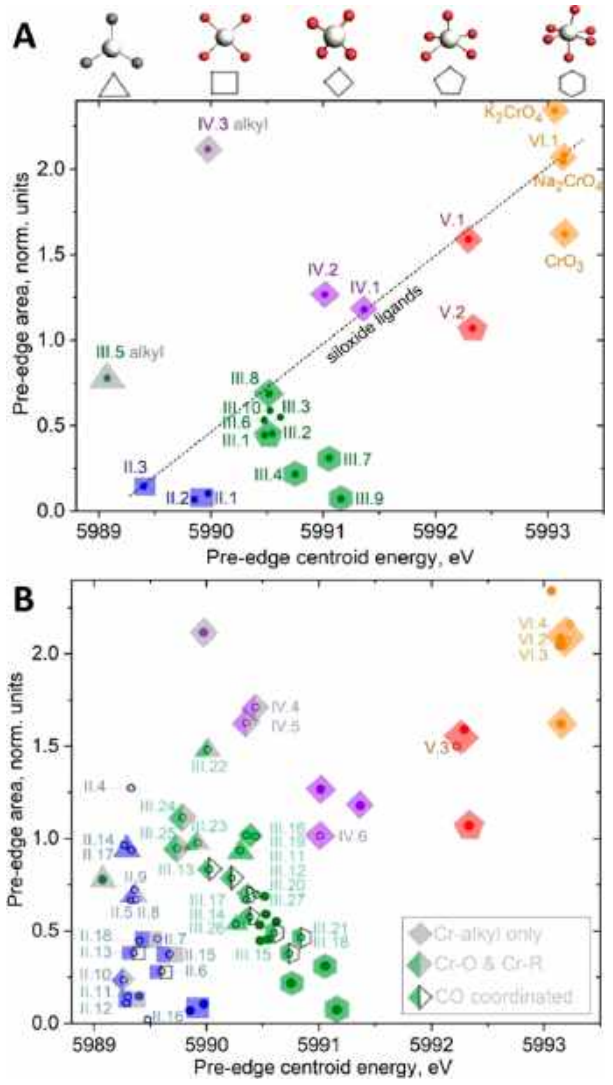

Figure 8. (A) 2D scatter plot with pre-edge areas and centroid energies extracted from the experimental XANES spectra of molecular Cr complexes (filled circles). The local coordination around Cr is marked as a polygon according to the corresponding legend on top (triangle = tricoordinated, square = square-planar, diamond = tetrahedral, pentagon = pentacoordinated; hexagon = hexacoordinated). The color coding represents the oxidation state (blue = Cr(II), green = Cr(III), purple = Cr(IV), red = Cr(V), and orange = Cr(VI)). Model complexes with siloxide ligands show a linear correlation in the pre-edge area with oxidation state when the coordination number remains unchanged. (B) Same as A but with additional data points from theoretically calculated spectra (hollow circles) as shown in Figure 9. Theoretically calculated values are calibrated based on the linear fit in Figure 7 prior to plotting on the same scale with experimental data points.

the dimensionality of each spectrum by extracting only the most informative features, i.e., appropriate spectral descriptors.[27]

Figure 6 describes several possible choices of descriptors, including the edge energy, the energy and the intensity of the main maximum, the lowest pit energy, the pre-edge area and the pre-edge centroid energy, and the intensity $\mu(E)$ of the pre-edge maximum. Combining two or three descriptors together can already provide relevant information about oxidation states, interatomic distances, and ligand types. Calculations can systematically differ from experimental results due to limitations in the theoretical approximations and convolutions or due to experimental artifacts. The benefit of using descriptors instead of the entire XANES spectra is their calibration ability. In Figure 7, we compare pre-edge areas and centroid energies evaluated from experimental reference spectra and theoretical simulations (see Section 2.3 of the SI for detailed information on the baseline fits and Figures S10 and S11 for correlations between pre-edge descriptors).

The linear calibration accounts for the systematic theoretical pre-edge energy offset and the underestimation of pre-edge areas in experimental spectra due to the overlap with the rising edge. This calibration curve is further applied for Cr K-edge theoretical XANES spectra and allows combining the experimental database of molecular references with theoretical spectra of possible active sites that are not readily obtained via molecular chemistry. Figure 8A shows a 2D scatter plot for pre-edge areas and centroid energies derived from experimental spectra. Both area and position of the pre-edge increase with increasing oxidation state. Within the same oxidation state, pre-edge intensities are most pronounced for tetrahedral environments and decrease from C_{4v} to D_{3h} and O_h symmetries due to the decrease of the 3d−4p hybridization at Cr. Complexes with alkyl ligands (**III.5** and **IV.3**) deviate from the general trend and show significantly lower pre-edge energies. The dotted line indicates an almost linear correlation of the pre-edge area with respect to the oxidation state, provided that the type of ligand (siloxide) and the coordination number remain unchanged. For pseudo-tetrahedral complexes (**III.8**, **IV.1**, **V.1**, and **VI.1**), this is explained by a decrease in the formal d-electron count at Cr, making more d orbitals accessible for electron transitions from the 1s orbital.

We complemented the series of experimental complexes with Cr(II−VI) silicates of different geometries,[21a,28] chroma-siloxane ring sizes, coordination numbers, and oxygenated byproducts in the presence or absence of ethylene. Low-coordinate Cr(II−IV) silicates with one or two alkyl groups are also considered here. Such DFT-optimized structures account for potential surface sites that are proposed to be present on silica surfaces but not really accessible via molecular chemistry.[1b,2c,d,g,h,5b,29] We also included the corresponding structures coordinated with CO to account for potential surface sites in the prereduced Phillips catalyst P2 as shown in Figure 9. Figure 8B shows the combined map including both experimental and theoretical structures. The trends observed in Figure 8A are also valid for the theoretical data set. Complexes with σ-donating alkyl ligands have a higher pre-edge intensity and a lower pre-edge centroid energy (compare **IV.4** and **IV.5** with **IV.6** or **III.24** and **III.25** with **III.13**). Pseudo-tetrahedral complexes have a higher pre-edge area than formally octahedral complexes (compare **III.13** and **III.18**). Some Cr(II) models with planar geometry, e.g., **II.4** and **II.14**, have large pre-edge areas and can be erroneously attributed to the Cr(III) oxidation state in Figure 8B. However, for planar complexes, the overlap between transitions to the Cr d states and the low-lying Cr $4p_z$ states can introduce uncertainties in the estimation of pre-edge areas. An example of such an overlap is clear for complex **III.5** in Figure 2B (see also the corresponding panel in Figure S17).

On the basis of the cross-validation, we have selected optimal descriptors for the combined data set of experimental and theoretical spectra and trained the Extra Trees[30] ML algorithm to classify the properties of the Cr complexes. The Extra Trees method does not suffer from overtraining and works well even for a small number of entries in the training set. The optimal number of randomized trees was adjusted between 40 and 200.

https://doi.org/10.1021/jacs.0c10791
J. Am. Chem. Soc. XXXX, XXX, XXX−XXX

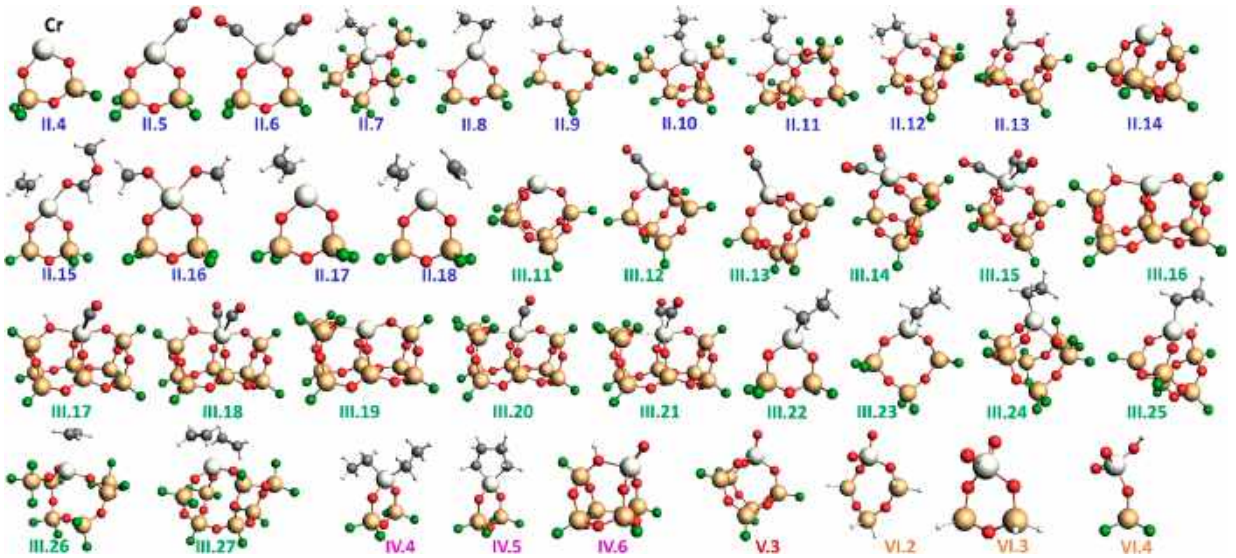

Figure 9. DFT-optimized structures of Cr(II−IV) surface silicates and potentially active sites as proposed in the literature to extend the series of synthesized molecular complexes. Cr atoms are marked in gray; C, dark gray; O, red; Si, yellow; F, green; and H, white. The silica surface was terminated by Si−F bonds (except for **VI.2** and **VI.3**, which are used as reported[29d]) including six- to 10-membered chroma-siloxane rings. Regarding the prereduced Phillips catalyst, P2, we also included low-valent Cr(II−III) complexes with CO ligands. Commonly proposed Cr(II−VI) active site structures, with or without ethylene and oxygenated byproducts, are also considered in this database. Note that the second ethylene molecule in structure **II.15** is weakly bound to Cr and therefore not shown in this plot. For simplicity, we used an ethyl fragment to indicate the growing polymer chain.

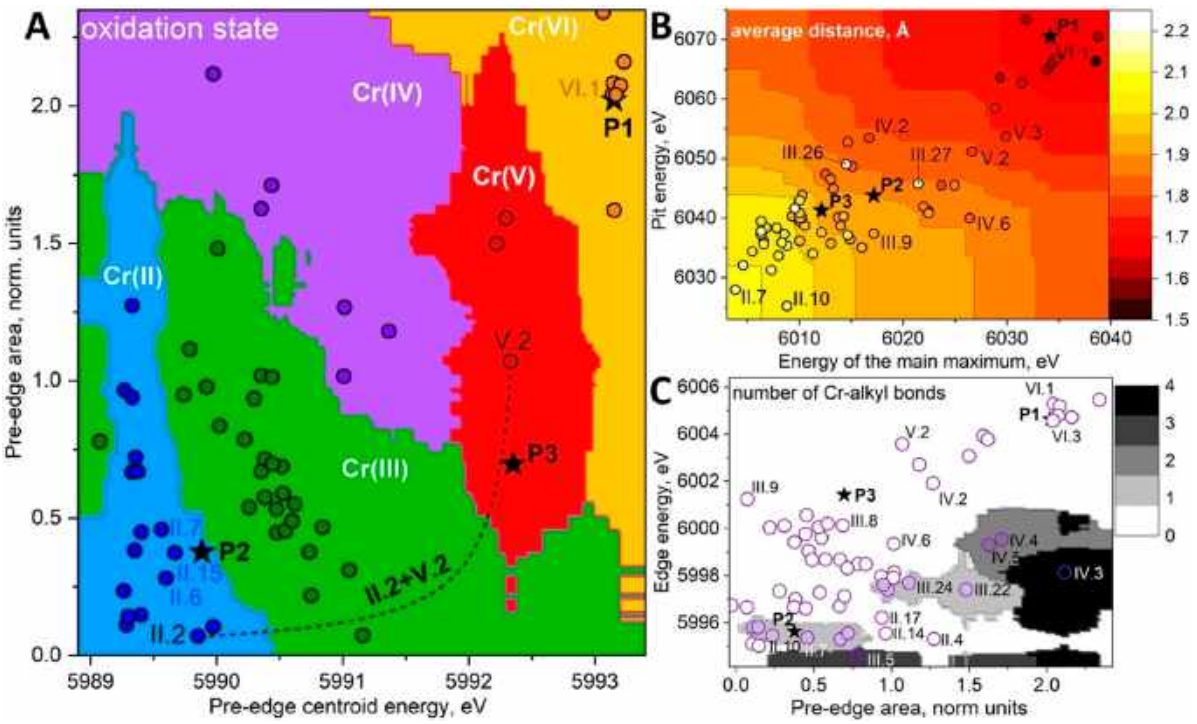

Figure 10. Extra Trees classification of the 2D space for the best pairs of pre-edge or near-edge descriptors based on the data set from Figure 8B. The experimental data from the Phillips catalyst at three different stages of the process (P1−P3) are projected onto each map (black stars). (A) Prediction of the Cr oxidation state based on the pre-edge centroid energy and the pre-edge area as descriptors. (B) Prediction of average Cr−X (X = O or C) distances in the first coordination sphere by using the energy of the main maximum of the XANES spectrum and the pit energy as descriptors. All dots are colored according to the mean distances. (C) Prediction of the quantity of Cr−alkyl bonds based on the pre-edge area and the edge energy.

Increasing the number of trees does not improve the quality. Figure 10 illustrates the performance of the ML classification by using 2D maps for the best pairs of descriptors in terms of their prediction quality. Qualitatively, if points for different classes are well separated on the 2D map, the chosen pair of descriptors is appropriate for classification. Figure 10A demonstrates the output of the Extra Trees algorithm which was trained on the data points from Figure 8B. The regions in the 2D map are classified in domains of Cr oxidation states with an overall prediction accuracy approaching 90%. The black stars (P1, P2,

https://doi.org/10.1021/jacs.0c10791
J. Am. Chem. Soc. XXXX, XXX, XXX−XXX

P3) in the 2D maps correspond to the descriptors determined from the experimental spectra for the freshly calcined (P1), the prereduced Phillips catalyst under CO (P2), and the freshly calcined Phillips catalyst in the presence of ethylene (P3). P1 and P2 are readily classified as Cr(VI) and Cr(II) silicates correspondingly.

The position of P3 belongs to the corner with low density of training points, and its formal assignment to Cr(V) is therefore not reliable. The lack of training points in this region is not surprising since a tetrahedral arrangement, with oxygen in the first coordination sphere, is the most abundant among Cr complexes in high oxidation state. Alternatively, P3 can be represented by a mixture of structures that differ in oxidation state and the local environment. The dotted line between complexes **II.2** and **V.2** indicates the evaluated pre-edge areas and centroid energies for linear combinations of two corresponding spectra. The curve is not linear since the pre-edge centroid energy varies nonlinearly in the sum of the linear combination of two pre-edge regions. This trace indicates that P3 can be represented, e.g., by a mixture of Cr(II) and Cr(V) silicates. Other linear combinations are also possible but omitted here for clarity. A more detailed analysis based on linear combination fitting for P1−P3 is described in the next section.

Another useful pair of spectral descriptors is shown in Figure 10B. The energy of the main maximum and the pit energy of the XANES spectrum are most sensitive to Cr−X (X = O or C) distances in the first coordination sphere. This choice of descriptors is not surprising and follows the semiempirical Natoli's rule.[31] Cr silicates with short bonds show higher main maxima and pit energies. By projecting the spectra of the Phillips catalyst on this map, we note that P3 and P2 are characterized by larger distances (∼1.9 Å), while P1 has an average Cr−O distance of about 1.7 Å.

In Figure 10C, we evaluated pre-edge areas and edge energies as the optimal pair of descriptors to determine the number of alkyl bonds. Cr complexes with several alkyl bonds are situated below the main diagonal and are characterized by larger pre-edge areas. At the same time, the edge energies are lower as compared to siloxide complexes with similar geometries (see Figure 2E for comparison). P1 and P3 are located well above the main diagonal of this graph. The presence of alkyl bonds in the freshly calcined Phillips catalyst (P1) and the catalyst under working conditions (P3) can therefore be excluded. This is expected for P1 but rather surprising for P3, suggesting that the fraction of catalytically active Cr-alkyl species is low and not detected. P2, the Phillips catalyst exposed to CO, may be assigned to a model structure with one alkyl bond, likely due to the presence of a fraction of Cr-silicates with CO ligands bound to it after reduction, as evidenced by IR.[5a]

We note several outliers in Figure 10. The first point corresponds to the structure **III.5** in the left green region of Figure 10A. The three alkyl ligands bound to Cr atom reduce the pre-edge centroid energy with respect to the other Cr(III) structures with alkoxide and siloxide ligands. The two white circles near P2 in Figure 10B are classified to the region with a 1.9 Å distance, but the corresponding structures (**III.26** and **III.27**) formally have average distances larger than 2.1 Å. These structures contain short Cr−O bonds together with weakly coordinated ethylene molecules in the first coordination sphere, making an appropriate classification difficult. Several outliers are also present in Figure 10C. The structures with a planar coordination sphere around Cr, for example, **II.4**, **II.14**, and **II.17**, contain a shoulder on the rising edge that affects the edge position and can overlap with the pre-edge region (see also the corresponding panels in Figure S18). To overcome uncertainties in the classification, the number of descriptors applied for training the ML algorithm can be increased.

Two-dimensional scatter plots are useful for the qualitative classification of unknown spectra. ML algorithms can offer a better quality of analysis based on any quantity of descriptors. Table 1 reports the quality of prediction for oxidation states, average distances in the first coordination sphere, and the number of Cr−alkyl bonds, based on three optimal pre-edge or near-edge descriptors of the XANES spectrum. The pre-edge region of the spectrum is sufficient to predict the Cr oxidation state and the number of alkyl bonds, while higher energy features of the XANES spectrum provide a better accuracy for the distance analysis. The use of alternative descriptors for the prediction of structural parameters is discussed in Section 4.2 of the SI.

Table 1. Prediction Accuracy (%) for Oxidation States and Other Structural Parameters of Cr Complexes by Using a Combination of Three Optimal Pre-Edge Descriptors (A, Area; B, Centroid Energy; C, $\mu(E)$ Max.) or Three Near-Edge Descriptors (D, Main Max. Energy; E, Pit Energy; F, Edge Slope)[a]

prediction accuracy (%)	[A, B, C]	[D, E, F]
oxidation state	**90**	67
number of alkyl bonds	**87**	77
average Cr−X distance	74	**90**

[a]The energy of the rising edge correlates with the pre-edge centroid energy and is therefore indirectly included in the analysis. For the oxidation state and the number of alkyl bonds, the 10-fold cross-validation is used to estimate the accuracy, while the R^2 (coefficient of determination) regression score function is evaluated for the average distance.

Applying the Linear Combination Analysis to the Phillips Catalyst. Industrially prepared Phillips catalysts under working conditions contain a mixture of different surface sites with a generally low number of active sites. To quantify the distribution of Cr sites with different oxidation states, we used a linear combination fit (LCF) of descriptors of the reference spectra. Selected descriptors of the near-edge region contain only important information from the spectrum, can be corrected for systematic differences between theoretical and experimental references (see Figure 7), and have high predictive power (see Table 1). In this section, we compare the results from the LCF of descriptors to the ML prediction together with a classical LCF applied to the pre-edge only and the full XANES spectrum with excluded pre-edge features.

In the first step, the descriptors are extracted from the experimental spectra of the Phillips catalyst at three different stages of the process (see Figure 11 and Table 2). In a second step, we construct linear combinations of all pairs of spectra in the library and vary their concentrations. In a third step the descriptors are evaluated for every entry in the library of mixtures. In the mixture, the pre-edge area varies linearly along with the concentration of two components, while the pre-edge centroid energy depends nonlinearly on the concentration (see for example the dotted line in Figure 10A). Finally, the database of descriptors of mixtures can be used for training the ML algorithm, or in the LCF by minimizing the L2 norm, with the set of descriptors as shown in Figure 6. Similar to the spectra in

https://doi.org/10.1021/jacs.0c10791
J. Am. Chem. Soc. XXXX, XXX, XXX−XXX

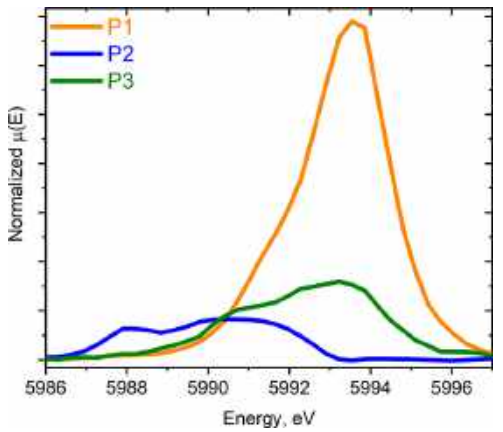

Figure 11. Pre-edge region of the Cr K-edge XANES spectra of the Phillips catalysts after baseline subtraction: P1, freshly calcined; P2, after prereduction with CO; P3, after calcination and ethylene exposure at 110 °C. All raw data were kindly provided by Groppo and collaborators as originally published.[5a]

Table 2. Calculated Descriptors from Experimental Spectra of the Phillips Catalysts That Are Used in the Linear Combination Fit

descriptor	P1	P2	P3
pre-edge area	2.02	0.38	0.70
pre-edge centroid (eV)	5993.15	5989.88	5992.35
pre-edge $\mu(E)$ max.	0.69	0.08	0.16

the database of the descriptors, all entries are normalized. Normalization implies subtracting the average and dividing each value by its standard deviation for each type of descriptors. Scheme 1 describes the procedure of the LCF.

The results from the LCF analysis for P1−P3 are visualized in Figure 12. Each square in Figure 12 corresponds to a best fit using a mixture of two reference spectra with given Cr oxidation

Scheme 1. Procedure for Finding the Optimal Concentrations of Components in the LCF by Using the Three Pre-Edge Descriptors (Area, Centroid Energy, and $\mu(E)$ Max.)[a]

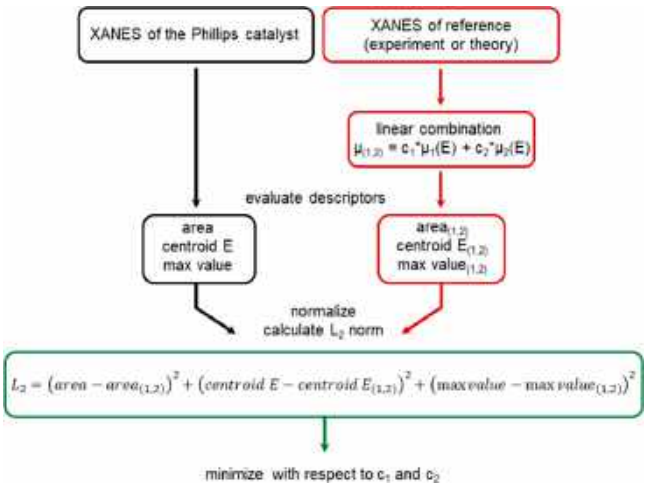

[a]A quantitative comparison between the sum of two reference spectra and the spectrum of the Phillips catalyst is performed by using the descriptors from Table 1.

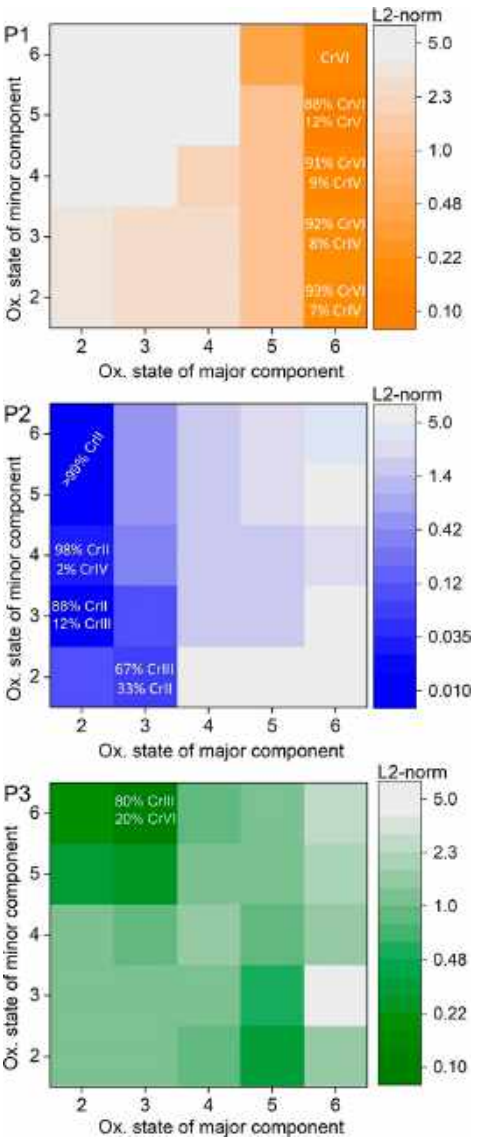

Figure 12. Results from the two-component LCF applied to the industrially prepared Phillips catalysts P1, P2, and P3 based on the procedure outlined in Scheme 1. The cells with the small L2 norm that cannot be distinguished within the uncertainty of the three pre-edge descriptors are labeled with their corresponding fractions of oxidation states. To achieve the best fit for a selected pair of oxidation states, e.g., (3,6), we made a loop over all possible pairs of reference spectra with given oxidation states, namely 3 and 6, and varied concentrations in the mixture until the L2 norm was minimized. An LCF analysis of the full XANES spectrum was necessary to exclude the cells (2,2) and (3,3) in P2 and the combination (2,6) in P3 from the best fits.

states. The colors denote the value of the L2 norm between the descriptors from the Phillips catalyst and the mixture of two reference spectra. The horizontal axis shows the oxidation state of the major component in the mixture. As follows from Figure 12, the best fit for P1 is achieved by using reference spectra of Cr(VI) complexes (88%) with only minor contributions from Cr(V) sites (12%). The values of the L2 norm for all combinations in the right column are very close. We have constructed a series of artificial mixtures with similar concentrations to what we obtained in all good fits and estimated the average uncertainty in the L2 norm to be 0.03 (i.e., this is an average distance between the wrong pair of oxidation

https://doi.org/10.1021/jacs.0c10791
J. Am. Chem. Soc. XXXX, XXX, XXX−XXX

states and a true one; see Section 4.6 of the SI for details). In this regard, all combinations in the right column of Figure 12A cannot be distinguished with three pre-edge descriptors. However, the dominant contribution of Cr(VI) in all good fits is about 90%. This agrees with Figure 10A, where the spectrum of P1 has a similar pre-edge area and centroid energy to Cr(VI) reference complexes.

The pre-edge spectrum of P2 after prereduction with CO has low intensity and shifts to lower energies (see Table 2 and Figure 11). In Figure 10A, P2 is located near the border between Cr(II) and Cr(III) domains. The linear combination analysis indicates a majority of square-planar Cr(II) silicates. For P2, the average uncertainty in the L2 norm is evaluated to 0.03 (see Table S18). Therefore, Figure 12B contains several labeled cells that cannot be distinguished from the best fit. The combinations consisting of Cr(II)−Cr(II) and Cr(III)−Cr(III) sites with a small L2 norm in Figure 12B could be excluded from the range of possible solutions based on the LCF analysis of the full XANES spectrum. The pre-edge analysis for the Phillips catalysts treated with ethene, P3, is more complex due to the mutual influence of unreduced Cr(VI) silicates, reduced Cr silicates, and the possible presence of Cr alkyl species active in ethylene polymerization. According to Figure 10A, the centroid position is indicative for Cr(V) silicates, while the overall pre-edge area suggests low-valent Cr sites, indicating a mixture of sites (see the dotted line in Figure 10A between complex **II.2** and **V.2**). Clearly, a multicomponent analysis is therefore essential for a relevant classification of the Phillips catalyst under reaction conditions.

P3 is best described by a two-component mixture consisting of Cr(III) (80%) along with remaining Cr(VI) silicates (20%) based on the pre-edge descriptor analysis. A mixture of Cr(V) and Cr(II) silicates with Cr(V) being the major component is less favorable due to the higher L_2 norm, consistent with previous findings.[2h,32] Here, the average uncertainty in the L2 norm for the LCF analysis is evaluated as 0.04. This would require other possible solutions such as the Cr(II)−Cr(VI) combination in Figure 12C. The latter is discriminated when considering the full energy interval of the XANES spectrum for the analysis (see Section 4.6 of the SI for details).

Besides the LCF analysis, average oxidation states may be predicted by using the ML algorithm trained on the database of mixtures (in contrast to the training on pure compounds in Figure 10). Table 3 compares the average Cr oxidation state evaluated from the best fit of the classical LCF analysis for the pre-edge and the post-edge of the XANES spectrum. The results from the LCF analysis are compared to the ML-predicted average oxidation state. Therefore, Table 3 contains the output of two independent methods (linear combination fit and Extra Trees algorithm) and two independent regions of the spectrum (pre-edge and post-edge up to 100 eV). Each value is reported by a range that was estimated via the cross-validation approach when predicted oxidation states are compared to the known oxidation states for 50 random artificial mixtures (see also Section 4 of the SI for details).

Similar to oxidation states, we expanded the analysis to evaluate average Cr−X (X = O or C) distances and the number of alkyl bonds based on ML prediction and classical LCF analysis (see Section 4 of the SI and Tables S15 and S16). Average Cr−X distances from the classical LCF analysis of the full spectrum are ∼2 Å for P2 and 1.9 Å P3, where P1 shows significantly lower average distances around 1.7 Å, consistent with the results in Figure 10B and the presence of Cr(VI) dioxo species. On the basis of ML predictions, we obtained a similar trend (1.7 Å for P1, 1.95 Å for P2, and 1.9 Å for P3). The results from the LCF analysis show no contribution from alkyl bonds to P3 in the best fit, suggesting that the fraction of catalytically active Cr-alkyl species lies below 5%, since the detection limit of the LCF approach can be estimated around 5% (see Section 4.4 of the SI for details on the detection limit of the number of alkyl bonds). The ML algorithm trained on the three pre-edge descriptors suggests the presence of alkyl bonds in P2. This is in agreement with the classification in Figure 10C and likely due to the presence of a fraction of surface Cr-silicates bound to the strongly σ-donating CO ligands, formed upon reduction under CO, as evidenced by IR.

Inspecting the fit pairs with low L2 norms can provide additional evidence to elucidate the site distribution on silica. P1 is described by the monomeric Cr(VI) dioxo-model complex **VI.I** in the best fit pair. For P2, the major fraction is characterized by the square-planar surface site **II.6** with CO coordinated to Cr. For P3, the majority of sites are predicted as highly coordinated Cr(III) silicates (**III.4** or **III.7** in the best fit). This is not surprising since the reduction of Cr(VI) silicates in the presence of ethylene generates oxygenated byproducts that poison most of the Cr(III) sites on silica, leaving only a small fraction of unsaturated, likely Cr(III), sites that are active in ethylene polymerization.

Table 3. Average Cr Oxidation States from Several Independent Approaches: LCF Analysis of XANES Spectra (Pre-edge XANES Region [5985−5997 eV] and the Full XANES Spectrum [5980−6100 eV] Excluding Pre-edge), Pre-edge Descriptors (Area, Centroid Energy, and $\mu(E)$ max), and the Prediction by the Extra Trees Algorithm Trained on 10 000 Mixtures Composed Randomly from the Reference Library[a]

method of analysis	P1	P2	P3
LCF of descriptors	5.5−6.0	2.0−2.5	3.2−4.0
best pair for the LCF of descriptors	**VI.1**, **V.3**	**II.6**, **III.16**	**III.7**, **VI.1**
ML prediction for descriptors	5.7−6.0	2.1−2.7	3.2−3.8
LCF of XANES (pre-edge)	5.6−6.0	2.0−2.5	3.5−4.1
best pair for the LCF of the pre-edge	**VI.1**	**II.6**	**III.7**
	IV.6	**IV.2**	**VI.1**
ML prediction for XANES (pre-edge)	5.6−6.0	2.1−2.7	3.4−4.0
LCF of XANES (post-edge)	5.5−5.9	2.4−2.8	3.6−4.0
best pair for the LCF of the post-edge	Na_2CrO_4	**II.3**	**III.4**
	V.1	**IV.2**	**V.2**/**VI.2**
ML prediction for XANES (post-edge)	5.4−5.8	2.7−3.1	3.7−4.1

[a]Along with the reported best pair for each LCF, other combinations with a similar L2 norm and average Cr oxidation state exist (see Table S14). For P3 we obtained an equal L2 norm for the pairs **III.4**+**V.2** and **III.4**+**VI.2**, which are both reported. The range for the oxidation states was estimated separately for each method via the cross-validation.

CONCLUSIONS

Decoding Cr K-Edge XANES Spectra. Cr pre-edge features contain precious information regarding oxidation states, local environment, and ligand types. To extract this information, we synthesized a series of tailored molecular Cr complexes, recorded Cr K-edge XANES spectra, and modeled them within one-electron DFT and ligand field multiplet simulations. We showed that pre-edge centroid energies increase with the

https://doi.org/10.1021/jacs.0c10791
J. Am. Chem. Soc. XXXX, XXX, XXX−XXX

oxidation state. Strongly donating alkyl ligands significantly lower the pre-edge/edge position. Pre-edge intensities increase with oxidation state and the deviation from centrosymmetry. Very importantly, XANES spectra from planar complexes display an intense sharp shoulder originating from transitions to low-lying empty p_z orbitals that can easily lead to a misassignment of the Cr oxidation state upon the sole analysis of the edge position. Spin exchange interactions split the pre-edge by up to 1.5 eV and dominate over the crystal field splitting for Cr complexes with unpaired electrons in the d shell. The splitting increases with the number of unpaired electrons. Cr_2O_3, a commonly used Cr(III) reference material, has different pre-edge features as opposed to molecular Cr(III) references. The second pre-edge peak arise from interactions between Cr centers in the periodic crystal and can overlap with the pre-edge of molecular Cr(VI) complexes. Therefore, restricting the interpretation of XANES spectra to commercially available solid-state reference materials, such as Cr_2O_3, is highly misleading. This probably explains parts of the numerous debates regarding the proposed structures of surface (active) sites in heterogeneous catalysis and the Phillips catalyst. Overall, we demonstrated the critical need of developing experimental or alternatively computational libraries of molecularly defined environments to fully grasp the origin of pre-edge and edge XANES features in surface sites, where coordination geometries likely defer from bulk structures.

Limitation of XANES and Resulting Controversies in Assigning Cr(II) and Cr(III) Oxidation States in the Phillips Catalysts. The ambiguity in assigning oxidation states to surface sites results from the sensitivity of different XAS regions itself. The limitations for using the pre-edge arises from the presence of an intense shoulder for square-planar Cr(II) and Cr(III) species or Cr sites with high and low pre-edge intensities, such as tetrahedral Cr(VI) and square-planar Cr(II) this situation is worsened by the ambiguity of the baseline subtraction in these cases. Furthermore, the presence of metal−carbon bonds in place of metal−oxygen bonds will lower the pre-edge centroid energy for a given oxidation state (see Figure 2). Thus, weak pre-edge features from six-coordinated Cr(III) species may overlap with Cr(II) pre-edge features if Cr-alkyl groups are present. This complicates the analysis of the Phillips catalyst under working conditions, and the full energy range of the XANES spectrum needs to be analyzed in parallel. In case the full XANES analysis fails to resolve the origin of the small fraction in a mixture, descriptors from other analytical methods (EPR shifts or XPS profile parameters for tailored complexes) may be added to the analysis via the described machine learning methodology.

The energy overlap of spectral features with high information content explains the difficulty in assigning XANES spectra to a combination of given oxidation states in the Phillips catalyst and thus the long-standing debates in the literature.

Supervised ML and LCF Analysis to Classify the Phillips Catalyst. The library of experimental and theoretical spectra provides a basis for supervised ML. We reduced the dimensionality of spectra in the database by extracting pre-edge descriptors. These descriptors help to correct for systematic differences between theoretical entries in the library compared to experimental data and thus use combined database to decipher the oxidation state of Cr in the Phillips catalyst at three stages of the process: after calcination (P1), after prereduction with CO (P2), and after reaction with ethylene (P3). The two-component analysis showed that the freshly calcined catalyst (P1) consists of mainly Cr(VI) dioxo silicates, while the prereduced catalyst (P2) contains square-planar Cr(II) silicates with a fraction of Cr(III) sites, in agreement with previous findings. The Phillips catalyst treated under ethylene consists mainly of highly coordinated Cr(III) silicates (∼80%) and unreduced Cr(VI) sites. Such species are likely not involved in polymerization. We do not find evidence for significant contributions from Cr(IV) sites, in contrast to what is proposed in the recent literature. Major contribution from Cr(II) sites may be also excluded if the full energy interval of XANES is analyzed. Catalytically active and low-coordinate Cr(III) sites with one alkyl bond may have overlapping pre-edge features with Cr(II) sites, and thus the sole use of a pre-edge XAS spectrum is not possible to isolate them. Within the proposed library of selected compounds, the fraction of low-coordinate Cr sites active in ethylene polymerization can be estimated below the detection limit of 5% when only single spectrum is used for analysis.

The choice of suitable descriptors based on the analysis of a series of tailored molecular complexes and ML is powerful and should be implemented as a standard approach. Extensions to the EXAFS region and complementary surface-specific techniques ~~(EPR and XPS)~~ are straightforward to analyze complex heterogeneous materials with a large distribution of surface sites. We are currently exploring this approach to understand the structure of surface sites of a broader range of heterogeneous catalysts.

METHODS

For the quantitative analysis, we chose three near-edge descriptors that are most sensitive to the Cr oxidation state. The pre-edge area, the pre-edge centroid energy, and the rising edge energy were calculated for each spectrum. The whole spectrum was fitted with an arctangent function (see Section 2.3 of the SI for more details) to calculate the edge position. A short region of the XANES spectrum near the pre-edge was also fitted with a baseline arctangent function, which was subtracted prior to the area and the centroid evaluation. To combine both descriptors from experimental and theoretical spectra, the latter were calibrated based on the data set of 18 molecular model complexes (see Figure 7). The calibration curve accounted for systematic differences between energy shifts and pre-edge areas and was also applied for the descriptors extracted from theoretically calculated XANES spectra of hypothetical surface sites. According to Figure 7, these differences are linear, in contrast to the behavior of other evaluated features, i.e., momentum of inertia of the pre-edge, which characterizes its spread. The origin of discrepancies in the energy shift for experimental and theoretical spectra arises from the DFT uncertainties for the core-level energies. The underestimation of experimental pre-edge areas arises from the overlap of the pre-edge peaks with the rising edge, while 1s−3d transitions in general can be isolated. We performed geometry optimizations for potential surface sites and pre-edge calculations within the DFT B3LYP level of theory using the QZ4P basis set as implemented in the ADF-2019 software (see Section 3 of the SI for more details). Theoretical pre-edge areas were evaluated in the region with large d-DOS contributions (see Figure S18 for more details) Therefore, some 1s−4p transitions can overlap with 1s−3d transitions in particular for planar complexes. Higher energy transitions were calculated within the finite difference method as implemented in the FDMNES software. While the XANES region is not discussed quantitatively in the present article, we use the full XANES spectrum for the edge energy evaluation. The ML analysis was performed by using the PyFitIt interface[33] inside the Jupyter notebooks (see Section 4 of the SI for more details). The linear combination fit for the three near-edge descriptors was performed as described above.

https://doi.org/10.1021/jacs.0c10791
J. Am. Chem. Soc. XXXX, XXX, XXX−XXX

■ ASSOCIATED CONTENT

Supporting Information

The Supporting Information is available free of charge at https://pubs.acs.org/doi/10.1021/jacs.0c10791.

Experimental details, material characterization data, and computational details (PDF)

Accession Codes

CCDC 2059701−2059706 contain the supplementary crystallographic data for this paper. These data can be obtained free of charge via www.ccdc.cam.ac.uk/data_request/cif, or by emailing data_request@ccdc.cam.ac.uk, or by contacting The Cambridge Crystallographic Data Centre, 12 Union Road, Cambridge CB2 1EZ, UK; fax: +44 1223 336033.

■ AUTHOR INFORMATION

Corresponding Authors

Olga V. Safonova − *Paul-Scherrer-Institute, CH-5232 Villigen, Switzerland;* orcid.org/0000-0002-6772-1414; Email: olga.safonova@psi.ch

Alexander A. Guda − *The Smart Materials Research Institute, Southern Federal University, Rostov-on-Don, Russia 344090;* orcid.org/0000-0002-6941-4987; Email: guda@sfedu.ru

Christophe Copéret − *Department of Chemistry and Applied Biosciences, ETH Zürich, CH-8093 Zürich, Switzerland;* orcid.org/0000-0001-9660-3890; Email: ccoperet@ethz.ch

Authors

David Trummer − *Department of Chemistry and Applied Biosciences, ETH Zürich, CH-8093 Zürich, Switzerland*

Keith Searles − *Department of Chemistry and Applied Biosciences, ETH Zürich, CH-8093 Zürich, Switzerland*

Alexander Algasov − *The Smart Materials Research Institute, Southern Federal University, Rostov-on-Don, Russia 344090; Institute of Mathematics, Mechanics and Computer Science, Southern Federal University, Rostov-on-Don, Russia 344090;* orcid.org/0000-0002-3222-1604

Sergey A. Guda − *The Smart Materials Research Institute, Southern Federal University, Rostov-on-Don, Russia 344090; Institute of Mathematics, Mechanics and Computer Science, Southern Federal University, Rostov-on-Don, Russia 344090;* orcid.org/0000-0002-2398-1847

Alexander V. Soldatov − *The Smart Materials Research Institute, Southern Federal University, Rostov-on-Don, Russia 344090*

Harry Ramanantoanina − *Paul-Scherrer-Institute, CH-5232 Villigen, Switzerland;* orcid.org/0000-0002-2086-6958

Complete contact information is available at: https://pubs.acs.org/10.1021/jacs.0c10791

Funding

The authors are grateful to the Swiss National Foundation (SNF) for financial support of this work (grant no. 200021_169134). A.G. and S.G. acknowledge the financial support from Russian Foundation for Basic Research (project number 20-32-70227).

Notes

The authors declare no competing financial interest.

■ ACKNOWLEDGMENTS

We acknowledge the Paul-Scherrer-Institute, Villigen, Switzerland, for provision of synchrotron radiation beam time at the Super XAS beamline (proposal #20180778) of the Swiss Light Source. We thank Dr. Ilia Moroz for assistance at the beamline and Dr. Murielle Delley for recording preliminary XANES data of molecular Cr complexes.[34] The authors greatly acknowledge Prof. Elena Groppo (University of Torino) for providing us the originally reported XANES spectra of the Phillips catalysts P1−P3.[5a] We also thank Dr. Michael Wörle (ETH Zürich) for assistance with crystallographic measurements, Dr. Thomas Gianetti for the initial synthesis of complex **III.7**, and Dr. Petr Sot for helpful discussions.

■ REFERENCES

(1) (a) Ruihua, C., Zhen, L., Lei, Z., Xuelian, H., Pengyuan, Q., Minoru, T., Moris, S. E., Susannah, L. S., Boping, L. Phillips Cr/Silica Catalyst for Ethylene Polymerization. In *Polyolefins: 50 Years after Ziegler and Natta I*; Kaminsky, W., Ed. Advances in Polymer Science Springer: Berlin, Heidelberg, 2013; Vol. *257*. (b) McDaniel, M. P. In *Advances in Catalyst*; Gates, B. C.; Knözinger, H., Eds.; Academic Press, 2010; Vol. *53*, Chapter 3, pp 123−606. (c) McDaniel, M. P. In *Handbook of Heterogeneous Catalysis*, 2nd ed.; Ertl, G.; Schüth, F.; Weitkamp, J., Eds.; Wiley-VCH Verlag GmbH & Co. KGaA: Weinheim, 2008; pp 3733−3792. (d) McDaniel, M. P. In *Advances in Catalysis*; Eley, D. D.; Pines, H.; Weisz, P. B., Eds.; Academic Press, 1985; Vol. 33, pp 47−98. (e) Sailors, H. R.; Hogan, J. P. History of Polyolefins. *J. Macromol. Sci., Chem.* **1981**, *15* (7), 1377−1402.

(2) (a) Cruz, C. A.; Monwar, M. M.; Barr, J.; McDaniel, M. P. Identification of the Starting Group on the First PE Chain Produced by the Phillips Catalyst. *Macromolecules* **2019**, *52* (15), 5750−5760. (b) Morra, E.; Martino, G. A.; Piovano, A.; Barzan, C.; Groppo, E.; Chiesa, M. In Situ X- and Q-Band EPR Investigation of Ethylene Polymerization on Cr/SiO2 Phillips Catalyst. *J. Phys. Chem. C* **2018**, *122* (37), 21531−21536. (c) Groppo, E.; Martino, G. A.; Piovano, A.; Barzan, C. The Active Sites in the Phillips Catalysts: Origins of a Lively Debate and a Vision for the Future. *ACS Catal.* **2018**, *8* (11), 10846−10863. (d) Gierada, M.; Handzlik, J. Active sites formation and their transformations during ethylene polymerization by the Phillips CrOx/SiO2 catalyst. *J. Catal.* **2017**, *352*, 314−328. (e) Brown, C.; Lita, A.; Tao, Y.; Peek, N.; Crosswhite, M.; Mileham, M.; Krzystek, J.; Achey, R.; Fu, R.; Bindra, J. K.; Polinski, M.; Wang, Y.; van de Burgt, L. J.; Jeffcoat, D.; Profeta, S.; Stiegman, A. E.; Scott, S. L. Mechanism of Initiation in the Phillips Ethylene Polymerization Catalyst: Ethylene Activation by Cr(II) and the Structure of the Resulting Active Site. *ACS Catal.* **2017**, *7* (11), 7442−7455. (f) Chakrabarti, A.; Gierada, M.; Handzlik, J.; Wachs, I. E. Operando Molecular Spectroscopy During Ethylene Polymerization by Supported CrOx/SiO2 Catalysts: Active Sites, Reaction Intermediates, and Structure-Activity Relationship. *Top. Catal.* **2016**, *59* (8-9), 725−739. (g) Fong, A.; Peters, B.; Scott, S. L. One-Electron-Redox Activation of the Reduced Phillips Polymerization Catalyst, via Alkylchromium(IV) Homolysis: A Computational Assessment. *ACS Catal.* **2016**, *6* (9), 6073−6085. (h) Brown, C.; Krzystek, J.; Achey, R.; Lita, A.; Fu, R.; Meulenberg, R. W.; Polinski, M.; Peek, N.; Wang, Y.; van de Burgt, L. J.; Profeta, S.; Stiegman, A. E.; Scott, S. L. Mechanism of Initiation in the Phillips Ethylene Polymerization Catalyst: Redox Processes Leading to the Active Site. *ACS Catal.* **2015**, *5* (9), 5574−5583. (i) Groppo, E.; Lamberti, C.; Bordiga, S.; Spoto, G.; Zecchina, A. The Structure of Active Centers and the Ethylene Polymerization Mechanism on the Cr/SiO2 Catalyst: A Frontier for the Characterization Methods. *Chem. Rev.* **2005**, *105* (1), 115−184. (j) Weckhuysen, B. M.; Wachs, I. E.; Schoonheydt, R. A. Surface Chemistry and Spectroscopy of Chromium in Inorganic Oxides. *Chem. Rev.* **1996**, *96* (8), 3327−3350. (k) Ghiotti, G.; Garrone, E.; Zecchina, A. IR investigation of polymerization centres of the phillips catalyst. *J. Mol. Catal.* **1988**, *46* (1-3), 61−77. (l) Yermakov, Y.; Zakharov, V. In

Advances in Catalysis; Eley, D. D.; Pines, H.; Weisz, P. B., Eds.; Academic Press, 1975; Vol. *24*, pp 173−219.

(3) (a) Bertagnolli, H.; Ertel, T. S. X-Ray Absorption Spectroscopy of Amorphous Solids, Liquids, and Catalytic and Biochemical Systems - Capabilities and Limitations. *Angew. Chem., Int. Ed. Engl.* **1994**, *33* (1), 45−66. (b) Bart, J. C. J.; Vlaic, G. In *Advances in Catalysis*; Eley, D. D.; Pines, H.; Weisz, P. B., Eds.; Academic Press, 1987; Vol. *35*, pp 1−138. (c) Lee, P. A.; Citrin, P. H.; Eisenberger, P.; Kincaid, B. M. Extended x-ray absorption fine structure—its strengths and limitations as a structural tool. *Rev. Mod. Phys.* **1981**, *53* (4), 769−806. (d) Bordiga, S.; Groppo, E.; Agostini, G.; van Bokhoven, J. A.; Lamberti, C. Reactivity of Surface Species in Heterogeneous Catalysts Probed by In Situ X-ray Absorption Techniques. *Chem. Rev.* **2013**, *113* (3), 1736−1850. (e) Zhong, L.; Lee, M.-Y.; Liu, Z.; Wanglee, Y.-J.; Liu, B.; Scott, S. L. Spectroscopic and structural characterization of Cr(II)/SiO2 active site precursors in model Phillips polymerization catalysts. *J. Catal.* **2012**, *293*, 1−12. (f) Gianolio, D.; Groppo, E.; Vitillo, J. G.; Damin, A.; Bordiga, S.; Zecchina, A.; Lamberti, C. Direct evidence of adsorption induced CrII mobility on the SiO2 surface upon complexation by CO. *Chem. Commun.* **2010**, *46* (6), 976−978. (g) Demmelmaier, C. A.; White, R. E.; van Bokhoven, J. A.; Scott, S. L. Nature of ≡SiOCrO2Cl and (≡SiO)2CrO2 Sites Prepared by Grafting CrO2Cl2 onto Silica. *J. Phys. Chem. C* **2008**, *112* (16), 6439−6449. (h) Groppo, E.; Prestipino, C.; Cesano, F.; Bonino, F.; Bordiga, S.; Lamberti, C.; Thüne, P. C.; Niemantsverdriet, J. W.; Zecchina, A. In situ, Cr K-edge XAS study on the Phillips catalyst: activation and ethylene polymerization. *J. Catal.* **2005**, *230* (1), 98−108. (i) Weckhuysen, B. M.; Schoonheydt, R. A.; Jehng, J.-M.; Wachs, I. E.; Cho, S. J.; Ryoo, R.; Kijlstra, S.; Poels, E. Combined DRS−RS−EXAFS−XANES−TPR study of supported chromium catalysts. *J. Chem. Soc., Faraday Trans.* **1995**, *91* (18), 3245−3253. (j) Wang, Y.; Ohishi, Y.; Shishido, T.; Zhang, Q.; Yang, W.; Guo, Q.; Wan, H.; Takehira, K. Characterizations and catalytic properties of Cr-MCM-41 prepared by direct hydrothermal synthesis and template-ion exchange. *J. Catal.* **2003**, *220* (2), 347−357. (k) Pak, C.; Haller, G. L. Reversible coordination change of chromium in Cr-MCM-41 and Cr-MCM-48 studied by X-ray absorption near edge structure. *Microporous Mesoporous Mater.* **2001**, *48* (1-3), 165−170. (l) Juhin, A.; Calas, G.; Cabaret, D.; Galoisy, L.; Hazemann, J.-L. Structural relaxation around substitutional Cr(III) in MgAl2O4. *Phys. Rev. B: Condens. Matter Mater. Phys.* **2007**, *76* (5), 054105. (m) Pantelouris, A.; Modrow, H.; Pantelouris, M.; Hormes, J.; Reinen, D. The influence of coordination geometry and valency on the K-edge absorption near edge spectra of selected chromium compounds. *Chem. Phys.* **2004**, *300* (1), 13−22. (n) Jousseaume, C.; Vivien, D.; Kahn-Harari, A.; Derouet, J.; Ribot, F.; Villain, F. Spectroscopic characterization of chromium (IV, V, VI) in Cr:Li2MSiO4 (M = Mg,Zn). *J. Appl. Phys.* **2003**, *93* (10), 6006−6015. (o) Jousseaume, C.; Ribot, F.; Kahn-Harari, A.; Vivien, D.; Villain, F. XAS study of chromium in Li2MSiO4 (M = Mg, Zn). *Nucl. Instrum. Methods Phys. Res., Sect. B* **2003**, *200*, 425−431. (p) Arcon, I.; Mirtic, B.; Kodre, A. Determination of Valence States of Chromium in Calcium Chromates by Using X-ray Absorption Near-Edge Structure (XANES) Spectroscopy. *J. Am. Ceram. Soc.* **1998**, *81* (1), 222−224. (q) Garcia, J.; Benfatto, M.; Natoli, C. R.; Bianconi, A.; Davoli, I.; Marcelli, A. Three particle correlation function of metal ions in tetrahedral coordination determined by XANES. *Solid State Commun.* **1986**, *58* (9), 595−599.

(4) (a) Sattler, J. J. H. B.; Ruiz-Martinez, J.; Santillan-Jimenez, E.; Weckhuysen, B. M. Catalytic Dehydrogenation of Light Alkanes on Metals and Metal Oxides. *Chem. Rev.* **2014**, *114* (20), 10613−10653. (b) Weckhuysen, B. M.; Schoonheydt, R. A.; Mabbs, F. E.; Collison, D. Electron paramagnetic resonance of heterogeneous chromium catalysts. *J. Chem. Soc., Faraday Trans.* **1996**, *92* (13), 2431−2436. (c) Weckhuysen, B. M.; De Ridder, L. M.; Grobet, P. J.; Schoonheydt, R. A. Redox Behavior and Dispersion of Supported Chromium Catalysts. *J. Phys. Chem.* **1995**, *99* (1), 320−326. (d) Weckhuysen, B. M.; Verberckmoes, A. A.; Buttiens, A. L.; Schoonheydt, R. A. Diffuse reflectance spectroscopy study of the thermal genesis and molecular structure of chromium-supported catalysts. *J. Phys. Chem.* **1994**, *98* (2), 579−584. (e) Hercules, D. M.; Proctor, A.; Houalla, M. Quantitative Analysis of Mixed Oxidation States in Supported Catalysts. *Acc. Chem. Res.* **1994**, *27* (12), 387−393. (f) Weckhuysen, B. M.; De Ridder, L. M.; Schoonheydt, R. A. A quantitative diffuse reflectance spectroscopy study of supported chromium catalysts. *J. Phys. Chem.* **1993**, *97* (18), 4756−4763.

(5) (a) Barzan, C.; Piovano, A.; Botavina, M.; Martino, G. A.; Agostini, G.; Martra, G.; Groppo, E. Exploring the benefits beyond the pre-reduction in methane of the Cr/SiO_2 Phillips catalyst: The molecular structure of the Cr sites and their role in the catalytic performance. *J. Catal.* **2019**, *373*, 173−179. (b) Barzan, C.; Piovano, A.; Braglia, L.; Martino, G. A.; Lamberti, C.; Bordiga, S.; Groppo, E. Ligands Make the Difference! Molecular Insights into CrVI/SiO2 Phillips Catalyst during Ethylene Polymerization. *J. Am. Chem. Soc.* **2017**, *139* (47), 17064−17073.

(6) Chakrabarti, A.; Wachs, I. E. The Nature of Surface CrOx Sites on SiO2 in Different Environments. *Catal. Lett.* **2015**, *145* (4), 985−994.

(7) Zecchina, A.; Garrone, E.; Ghiotti, G.; Morterra, C.; Borello, E. Chemistry of silica supported chromium ions. I. Characterization of the samples. *J. Phys. Chem.* **1975**, *79* (10), 966−972.

(8) Tromp, M.; Moulin, J.; Reid, G.; Evans, J. Cr K-Edge XANES Spectroscopy: Ligand and Oxidation State Dependence — What is Oxidation State? *AIP Conf. Proc.* **2006**, *882* (1), 699−701.

(9) Glatzel, P.; Smolentsev, G.; Bunker, G. the electronic structure in 3d transition metal complexes: Can we measure oxidation states? *Journal of Physics: Conference Series* **2009**, *190*, 012046.

(10) (a) Shimizu, K.-i.; Maeshima, H.; Yoshida, H.; Satsuma, A.; Hattori, T. Ligand field effect on the chemical shift in XANES spectra of Cu(II) compounds. *Phys. Chem. Chem. Phys.* **2001**, *3* (5), 862−866. (b) Westre, T. E.; Kennepohl, P.; DeWitt, J. G.; Hedman, B.; Hodgson, K. O.; Solomon, E. I. A Multiplet Analysis of Fe K-Edge 1s → 3d Pre-Edge Features of Iron Complexes. *J. Am. Chem. Soc.* **1997**, *119* (27), 6297−6314.

(11) Wilke, M.; Farges, F.; Petit, P.-E.; Brown, G. E., Jr.; Martin, F. Oxidation state and coordination of Fe in minerals: An Fe K-XANES spectroscopic study. *Am. Mineral.* **2001**, *86* (5-6), 714−730.

(12) (a) Zheng, C.; Chen, C.; Chen, Y.; Ong, S. P. Random Forest Models for Accurate Identification of Coordination Environments from X-Ray Absorption Near-Edge Structure. *Patterns* **2020**, *1* (2), 100013. (b) Carbone, M. R.; Topsakal, M.; Lu, D.; Yoo, S. Machine-Learning X-Ray Absorption Spectra to Quantitative Accuracy. *Phys. Rev. Lett.* **2020**, *124* (15), 156401. (c) Liu, Y.; Marcella, N.; Timoshenko, J.; Halder, A.; Yang, B.; Kolipaka, L.; Pellin, M. J.; Seifert, S.; Vajda, S.; Liu, P.; Frenkel, A. I. Mapping XANES spectra on structural descriptors of copper oxide clusters using supervised machine learning. *J. Chem. Phys.* **2019**, *151* (16), 164201. (d) Carbone, M. R.; Yoo, S.; Topsakal, M.; Lu, D. Classification of local chemical environments from x-ray absorption spectra using supervised machine learning. *Physical Review Materials* **2019**, *3* (3), 033604. (e) Timoshenko, J.; Lu, D.; Lin, Y.; Frenkel, A. I. Supervised Machine-Learning-Based Determination of Three-Dimensional Structure of Metallic Nanoparticles. *J. Phys. Chem. Lett.* **2017**, *8* (20), 5091−5098.

(13) Conley, M. P.; Delley, M. F.; Siddiqi, G.; Lapadula, G.; Norsic, S.; Monteil, V.; Safonova, O. V.; Copéret, C. Polymerization of Ethylene by Silica-Supported Dinuclear CrIII Sites through an Initiation Step Involving C-H Bond Activation. *Angew. Chem., Int. Ed.* **2014**, *53* (7), 1872−1876.

(14) Edema, J. J. H.; Gambarotta, S.; Van Bolhuis, F.; Smeets, W. J. J.; Spek, A. L. New classes of monomeric and dimeric square-planar chromium(II) aryloxides: syntheses and structures. *Inorg. Chem.* **1989**, *28* (7), 1407−1410.

(15) Ocone, L. P.; Block, B.; Collman, P. A.; Buckingham, D. Anyhdrous Chromium(II) Acetate, Chromium(II) Acetate 1-Hydrate, & Bis(2,4-Pentanedionato)Chromium (II). *In Inorganic Syntheses* **2007**, 125−132.

(16) Ciborska, A.; Chojnacki, A.; Wojnowski, W. Bis(tetrahydrofuran-[kappa]O)tris(tri-tert-butoxysiloxy)chromium(III). *Acta Crystallogr., Sect. E: Struct. Rep. Online* **2007**, *63* (4), m1103−m1104.

https://doi.org/10.1021/jacs.0c10791
J. Am. Chem. Soc. XXXX, XXX, XXX−XXX

(17) Konig, S. N.; Maichle-Mossmer, C.; Tornroos, K. W.; Anwander, R. Siloxide Complexes of Chromium(II), Manganese(II), Cobalt(II), and Chromium(III) Incorporating Potassium(I). *Z. Naturforsch., B: J. Chem. Sci.* **2014**, *69* (11-12), 1375−1383.
(18) Herrmann, W. A.; Huber, N. W.; Anwander, R.; Priermeier, T. Monomere flüchtige Alkoxide von Chrom und Bismut. *Chem. Ber.* **1993**, *126* (5), 1127−1130.
(19) Barker, G. K.; Lappert, M. F.; Howard, J. A. K. Silylmethyl and related complexes. Part 6. Preparation, properties, and crystal and molecular structure of tris[bis(trimethylsilyl)methyl]-chromium-(III);the chemistry of related compounds of titanium(III), vanadium-(III), zirconium(IV), and hafnium(IV). *J. Chem. Soc., Dalton Trans.* **1978**, No. 7, 734−740.
(20) Thaler, E. G.; Rypdal, K.; Haaland, A.; Caulton, K. G. Structure and reactivity of chromium(4+) tert-butoxide. *Inorg. Chem.* **1989**, *28* (12), 2431−2434.
(21) (a) Schulzke, C.; Enright, D.; Sugiyama, H.; LeBlanc, G.; Gambarotta, S.; Yap, G. P. A.; Thompson, L. K.; Wilson, D. R.; Duchateau, R. The Unusual Stability of Homoleptic Di- and Tetravalent Chromium Alkyls. *Organometallics* **2002**, *21* (18), 3810−3816. (b) Mowat, W.; Shortland, A. J.; Hill, N. J.; Wilkinson, G. Elimination stabilized alkyls. Part II. Neopentyl and related alkyls of chromium(IV). *J. Chem. Soc., Dalton Trans.* **1973**, No. 7, 770−778.
(22) Krumpolc, M.; Rocek, J. Synthesis of stable chromium(V) complexes of tertiary hydroxy acids. *J. Am. Chem. Soc.* **1979**, *101* (12), 3206−3209.
(23) de Groot, F.; Vankó, G.; Glatzel, P. The 1s x-ray absorption pre-edge structures in transition metal oxides. *J. Phys.: Condens. Matter* **2009**, *21* (10), 104207.
(24) (a) Ramanantoanina, H. A DFT-based theoretical model for the calculation of spectral profiles of lanthanide M4,5-edge x-ray absorption. *J. Chem. Phys.* **2018**, *149* (5), 054104. (b) Ramanantoanina, H.; Daul, C. A non-empirical calculation of 2p core-electron excitation in compounds with 3d transition metal ions using ligand-field and density functional theory (LFDFT). *Phys. Chem. Chem. Phys.* **2017**, *19* (31), 20919−20929.
(25) Friedman, R.; Ronald, A. Atomic Spectra and Atomic Structure. In *Molecular Quantum Mechanics*, 5th ed.; Oxford University Press Inc.: New York, 2011; pp 210−255.
(26) Timoshenko, J.; Wrasman, C. J.; Luneau, M.; Shirman, T.; Cargnello, M.; Bare, S. R.; Aizenberg, J.; Friend, C. M.; Frenkel, A. I. Probing Atomic Distributions in Mono- and Bimetallic Nanoparticles by Supervised Machine Learning. *Nano Lett.* **2019**, *19* (1), 520−529.
(27) Torrisi, S. B.; Carbone, M. R.; Rohr, B. A.; Montoya, J. H.; Ha, Y.; Yano, J.; Suram, S. K.; Hung, L. Random forest machine learning models for interpretable X-ray absorption near-edge structure spectrum-property relationships. *npj Comput. Mater.* **2020**, *6* (1), 109.
(28) (a) Zeng, Y.; Liu, S.; Terano, M. Silsesquioxane-Supported Chromium Catalyst for Insight into Phillips-Type Ethylene Polymerization. *Macromol. React. Eng.* **2018**, *12* (5), 1800049. (b) Liu, H.-J.; Cai, I. C.; Fedorov, A.; Ziegler, M. S.; Copéret, C.; Tilley, T. D. Tricoordinate Organochromium(III) Complexes Supported by a Bulky Silylamido Ligand Produce Ultra-High-Molecular Weight Polyethylene in the Absence of Activators. *Helv. Chim. Acta* **2016**, *99* (11), 859−867. (c) MacAdams, L. A.; Buffone, G. P.; Incarvito, C. D.; Rheingold, A. L.; Theopold, K. H. A Chromium Catalyst for the Polymerization of Ethylene as a Homogeneous Model for the Phillips Catalyst. *J. Am. Chem. Soc.* **2005**, *127* (4), 1082−1083. (d) Ikeda, H.; Monoi, T.; Sasaki, Y. Performance of the Cr[CH(SiMe3)2]3/SiO2 catalyst for ethylene polymerization compared with the performance of the Phillips catalyst. *J. Polym. Sci., Part A: Polym. Chem.* **2003**, *41* (3), 413−419. (e) Blom, R.; Swang, O. Dynamic Behaviour of Tris(2-methylallyl)chromium - NMR and DFT Results. *Eur. J. Inorg. Chem.* **2002**, *2002* (2), 411−415. (f) Bade, O. M.; Blom, R.; Ystenes, M. Chromium Allyls on Silica: A Study of Structure and Reactivity. *Organometallics* **1998**, *17* (12), 2524−2533.
(29) (a) Floryan, L.; Borosy, A. P.; Núñez-Zarur, F.; Comas-Vives, A.; Copéret, C. Strain effect and dual initiation pathway in CrIII/SiO2 polymerization catalysts from amorphous periodic models. *J. Catal.* **2017**, *346*, 50−56. (b) Conley, M. P.; Delley, M. F.; Núñez-Zarur, F.; Comas-Vives, A.; Copéret, C. Heterolytic Activation of C-H Bonds on CrIII−O Surface Sites Is a Key Step in Catalytic Polymerization of Ethylene and Dehydrogenation of Propane. *Inorg. Chem.* **2015**, *54* (11), 5065−5078. (c) Delley, M. F.; Núñez-Zarur, F.; Conley, M. P.; Comas-Vives, A.; Siddiqi, G.; Norsic, S.; Monteil, V.; Safonova, O. V.; Copéret, C. Proton transfers are key elementary steps in ethylene polymerization on isolated chromium(III) silicates. *Proc. Natl. Acad. Sci. U. S. A.* **2014**, *111* (32), 11624−11629. (d) Demmelmaier, C. A.; White, R. E.; van Bokhoven, J. A.; Scott, S. L. Evidence for a chromasiloxane ring size effect in Phillips (Cr/SiO2) polymerization catalysts. *J. Catal.* **2009**, *262* (1), 44−56. (e) Gierada, M.; Handzlik, J. Computational insights into reduction of the Phillips CrOx/SiO2 catalyst by ethylene and CO. *J. Catal.* **2018**, *359*, 261−271.
(30) Geurts, P.; Ernst, D.; Wehenkel, L. Extremely randomized trees. *Machine Learning* **2006**, *63* (1), 3−42.
(31) Natoli, C. R. In *Distance Dependence of Continuum and Bound State of Excitonic Resonances in X-Ray Absorption Near Edge Structure (XANES)*; Springer: Berlin, Heidelberg, 1984. Hodgson, K. O.; Hedman, B.; Penner-Hahn, J. E., Eds. *EXAFS and Near Edge Structure III*; Springer: Berlin, Heidelberg, 1984; pp 38−42.
(32) (a) Myers, D. L.; Lunsford, J. H. Silica-supported chromium catalysts for ethylene polymerization: The active oxidation states of chromium. *J. Catal.* **1986**, *99* (1), 140−148. (b) Myers, D. L.; Lunsford, J. H. Silica-supported chromium catalysts for ethylene polymerization. *J. Catal.* **1985**, *92* (2), 260−271. (c) Beck, D. D.; Lunsford, J. H. The active site for ethylene polymerization over chromium supported on silica. *J. Catal.* **1981**, *68* (1), 121−131. (d) Przhevalskaya, L. K.; Shvets, V. A.; Kazansky, V. B. The study of active centers of ethylene polymerization over chromium catalysts prepared from tri- and bivalent chromium compounds. *J. Catal.* **1975**, *39* (3), 363−368.
(33) Martini, A.; Guda, S. A.; Guda, A. A.; Smolentsev, G.; Algasov, A.; Usoltsev, O.; Soldatov, M. A.; Bugaev, A.; Rusalev, Y.; Lamberti, C.; Soldatov, A. V. PyFitit: The software for quantitative analysis of XANES spectra using machine-learning algorithms. *Comput. Phys. Commun.* **2020**, *250*, 107064.
(34) Delley, M. F. *Molecular-Level Understanding of Structure and Reactivity of Isolated Chromium Sites on Oxide Surfaces*; ETH Zurich, 2017.

https://doi.org/10.1021/jacs.0c10791
J. Am. Chem. Soc. XXXX, XXX, XXX−XXX